Measurement of $\pi^+\pi^-$ Photoproduction in Double-Polarization Experiments using CLAS

L. Blaszczyk, S. Chen, P. Coltharp, V. Credé [1 2], P. Eugenio,
C. Hanretty, A. Ostrovidov, B. Sharin, B. Stokes
Florida State University, Tallahassee, FL 32306

M. Bellis [1], C. Meyer, R. Schumacher
Carnegie Mellon University, Pittsburgh, PA 15213

C. Djalali, O. Dzyubak, R. Gothe, S. Strauch [1], D. Tedeschi
University of South Carolina, Columbia, SC 29208

H. Crannell, F.J. Klein, J. Santoro, D.I. Sober
The Catholic University of America, Washington, DC 20064

D. Ireland, K. Livingston, G. Rosner, D. Protopopescu
University of Glasgow, Glasgow G12 8QQ, United Kingdom

V. Burkert, V. Mokeev, S. Stepanyan
Thomas Jefferson National Accelerator Facility, Newport News, VA 23606

G.V. Fedotov, B.S. Ishkhanov, E.L. Isupov, N.V. Shvedunov
Skobeltsyn Nuclear Physics Institute at Moscow State University,
119899 Moscow, Vorob'evy gory, Russia

R. Miskimen, M. Wood
University of Massachusetts, Amherst, MA 01003

J. Ball, P. Collins, M. Dugger, E. Pasyuk, B. Ritchie
Arizona State University, Tempe, AZ 85287-1504

B.L. Berman, W.J. Briscoe, Y.Y. Ilieva, P. Nadel-Turonski, I. Strakovsky, A. Tkabladze
The George Washington University, Washington, DC 20052

D. Watts
University of Edinburgh, Edinburgh EH9 3JZ, United Kingdom

P.L. Cole
Idaho State University, Pocatello, ID 83209

D. Jenkins
Virginia Polytechnic Institute and State University, Blacksburg, VA 24061

M. Khandaker
Norfolk State University, Norfolk, VA 23504

M.F. Vineyard
Union College, Schenectady, NY 12308

+ The CLAS Collaboration

December 5, 2005

[1] Co-Spokesperson
[2] Contact Person: crede@fsu.edu

Abstract

Polarization asymmetries are an essential ingredient in the interpretation of various meson production reactions in terms of the various resonances that contribute to the processes as real or virtual intermediate states. In the past, the $p\pi^+\pi^-$ final state has been treated often as arising from either of the quasi two-body states $\Delta\pi$ or $N\rho$, followed by the decay of the Δ or the ρ. This approach has been reasonably successful. With today's facilities running at all energies from threshold up to relatively high energies, a more complete determination and description of polarization observables for the three-body final state is warranted. It must be stressed that experiments with more than a single pseudoscalar in the final state have been touted as our best hope for finding the *missing* resonances. We consider it a top priority that the polarization observables for such processes be measured and elucidated in a more general framework, one that goes beyond the quasi two-body asumption. Partial wave analyses or other analyses based on isobar models show clearly the importance and the need of polarization observables since the analysis of unpolarized data often leads to ambiguous solutions. The closer we arrive at a *complete* experiment, the fewer ambiguities remain.

We propose to measure single and double-polarization observables in the photoproduction of two charged pions using the Hall-B photon-beam facility and the CLAS spectrometer which is a unique magnetic spectrometer with large acceptance. It allows operation of a transversely- as well as longitudinally-polarized frozen-spin target (FROST). We intend to measure three single-polarization observables ($\mathbf{P_x}$, $\mathbf{P_y}$, $\mathbf{P_z}$) and nine double-polarization observables ($\mathbf{P_x^{s,c}}$, $\mathbf{P_y^{s,c}}$, $\mathbf{P_z^{s,c}}$, $\mathbf{P_x^{\odot}}$, $\mathbf{P_y^{\odot}}$, $\mathbf{P_z^{\odot}}$) in the mass range up to 2 GeV/c^2. No additional beam time for two-pion production is required. However, we ask the PAC for the approval of the physical motivation for this reaction. Together with the experiments E02-112, E03-105, E04-102, and E05-012, we will provide essential new data of unprecedented quality and kinematical coverage suitable for coupled-channel analyses, i.e. one of the keys for progress in hadronic physics.

In addition, we propose to take data above 2 GeV/c^2. In this case, the physics motivated in this proposal requires 22 days of additional beam time in the framework of the whole FROST project. However, we are aware of the already approved 84 days for the above mentioned proposals and feel committed to prove the success of the project before requesting the full amount of additional beam time. Therefore, we ask the PAC for the approval of only 4 additional days of beam time for measurements using a circularly-polarized beam incident on a transversely-polarized target (determination of $\mathbf{P_x^{\odot}}$ and $\mathbf{P_y^{\odot}}$). These data will be taken at a higher CEBAF energy of 3.1 GeV and thus, the observables will cover the important mass region at and above 2 GeV/c^2. With these 4 days, we expect a statistical accuracy of 0.05, which will be sufficient to distinguish between different resonance contributions.

Studying $\pi^+\pi^-$ photoproduction provides answers to a large variety of questions. In the low-energy range for example, the $P_{11}(1440)$ (*Roper* Resonance) and its properties can be investigated. Our plan is to analyze the $\pi^+\pi^-$ data jointly with polarization data on single-pion photoproduction, which was proposed in E03-105 and E04-102. This will help to obtain a better understanding of the $P_{11}(1440)$. Furthermore at higher energies, a group of negative-parity Δ-states with masses around 1900 MeV can be studied for which only weak evidence exists so far. Their verification would be in contradiction with quark-model calculations predicting these states at significantly higher masses. Finally, the measurement of the helicity difference will determine the $\pi^+\pi^-$ contribution to the GDH integrand.

1 The CLAS Double-Polarization Program

The excited states of the nucleon cannot simply be inferred from cleanly separated spectral lines. Quite the contrary, a *spectral analysis* in nucleon resonance physics is complicated by the fact that the resonances are broadly overlapping states which decay into a multitude of final states involving mesons and baryons. In order to provide a consistent and complete picture of an individual nucleon resonance, the various possible production and decay channels must be treated in a multi-channel framework that permits separating resonance from background contributions. Very often, resonances reveal themselves more clearly through interference with dominant amplitudes. These interference terms can be isolated via polarization observables. However, in the absence of experimental data on polarization observables, in particular for multi-meson final states, the predictive power of currently used theoretical models is unclear.

Understanding the low-energy, or long-distance, properties of Quantum Chromodynamics (QCD) is a fascinating intellectual challenge. Hadrons are unique in that their masses are nearly 50 times greater than the bare masses of their constituents. The proposed activities for hadron spectroscopy are complementary to experimental studies of hadron structure (electroweak form factors, Forward and Generalized Parton Distributions). Both are essential for progress in this challenging subject.

Although many baryon resonances have been seen already in $\pi N \to \pi N$, ηN, $\pi\pi N$, ΛK, etc., many of these states cannot be considered well known. Difficult multi-channel analyses are required to find evidence for resonances from the data. Models based on three constituent quark degrees of freedom also predict more states than have been seen in the analyses, and there is a focused effort to discover evidence for as many as possible of these *missing* states in new data from the reactions $\gamma N \to \pi N$, $\pi\pi N$, ηN, ωN, $K\Lambda$, $K\Sigma$, etc.

At this point, it is important to emphasize that constituent quark models (CQMs) are currently the best approach to make predictions for masses, widths, and other decay properties of baryon states. Although these calculations serve only as a suggestion for how to tackle the challenges in hadron spectroscopy, they represent the only source of information for most observables which can be directly confronted with experimental findings. The level of agreement between the models and experiments is certainly very promising. However, other approaches are well on the way to predicting baryon properties based on first principles. Presumably within the next five years, given the latest progress in the field, more accurate predictions from lattice-QCD calculations will be available derived from a fundamental quantum field theory. At that time, it will be very important to have the necessary data at hand, which consequently have to be taken now. Eventually, the CQMs may become obsolete and for this reason this proposal is not seeking to test these models. Nevertheless, they play an important role in determining which physics regions should be explored and where exciting physics can be expected.

In strong interactions, rescattering effects are known to play an important role. A particular final state may rescatter and form another intermediate resonance which then decays and eventually leads to a different final state. The total amplitude for a given channel can thus be written as a coherent sum over all isobars and partial waves. For this reason, a large number of different final states must be studied, ultimately forming the input for a coupled-channel analysis. In addition to a multi-channel treatment of baryon data, polarization asymmetries are an essential ingredient in the interpretation of various meson production reactions in terms of the resonances that contribute to the processes, as real or virtual intermediate

states. In 2006, Hall-B at Jefferson Laboratory and the CB-ELSA Experiment at the e^- facility ELSA (Bonn, Germany) will provide polarization data in photoproduction which are presently not available. These two experiments form a complementary set of detectors to study baryon resonances by capitalizing on charged-particle and multi-photon (from the decay of neutral mesons) final states, respectively. The situation is unique and it is our scientific commitment to jump at this chance of combining the measurement of isospin-related reactions and to synchronize the corresponding analyses. Among many other well rated proposals, the proposal ELSA/6-2005 [1] on the *Measurement of Double-Polarization Observables in $2\pi^0$-Photoproduction with the Crystal-Barrel Detector at ELSA* obtained an A– rating and data taking is scheduled for 2006. The proposed systematic studies of single- as well as multi-meson final states will provide the first comprehensive data set of polarization observables and are necessary to experimentally assess nucleon structure.

At the time of this writing, four proposals to determine double-polarization observables are approved for experiments to run in Hall-B of Jefferson Lab, focussing on single-meson production [2, 3, 4, 5]. A brief description of these experiments will be given in the following three sections. The hitherto missing important piece is this proposal on the photoproduction of two charged pions, which will complete the picture. Ultimately, FROST will provide the data for real progress in this field.

Search for missing Nucleon Resonances in the Photoproduction of Hyperons using a Polarized-Photon Beam and a Polarized Target

The experiment E02-112 [2] will measure a large set of single and double-polarization observables in associated strangeness production. The final goal of this experiment, in concert with the CLAS-g1 experiment on hyperon photoproduction (E89-004) and the CLAS Approved Analysis of $\vec{\gamma}p \to \mathrm{K}^+\Lambda$ [6] (as part of CLAS-g8 [7, 8, 9]), is to perform a complete set of measurements for ground-state hyperon photoproduction in the reactions $\gamma p \to \mathrm{K}^+\Lambda$, $\gamma p \to \mathrm{K}^+\,\Sigma^0$, and $\gamma p \to \mathrm{K}^0\,\Sigma^+$. This will allow to perform a full partial wave analysis and to determine the contributing multipoles as a function of the center-of-mass energy.

Pion Photoproduction from a Polarized Target

The experiment E03-105 [3] intends to study single-pion photoproduction reactions, $\mathrm{p}(\gamma,\pi^+)\mathrm{n}$ and $\mathrm{p}(\gamma,\mathrm{p})\pi^0$, with a polarized beam and a longitudinally- as well as transversely-polarized target using the CLAS detector at Jefferson Lab Hall-B. The experiment will measure two single- (**T** and **P**) and three double-polarization observables (**G**, **F**, and **H**); experiment E01-104 will measure the double-polarization observable **E**. The data will greatly constrain partial wave analyses and reduce model-dependent uncertainties in the extraction of nucleon resonance properties, providing a new benchmark for comparisons with QCD-inspired models. The measurements will span $\cos(\theta_{\mathrm{cm}})$ from -0.9 to 0.9 in a center-of-mass energy range above 1300 MeV and up to 2150 MeV.

Measurement of Polarization Observables in η Photoproduction with CLAS

The experiment E05-012 [5] plans to measure the observables $\mathbf{\Sigma}$, **T**, **P**, **E**, **F**, **G**, and **H** in η photoproduction for photon energies between $0.75 - 2.0$ GeV. Special attention will be dedicated to the range of $W = 1.5 - 1.8$ GeV. The authors of this proposal anticipate 10 angular bins within $\cos(\theta_{\mathrm{cm}})$ from -0.9 to 0.9 and expect a statistical accuracy for all observables between $0.05 - 0.1$.

2 Introduction

The spectrum and properties of excited baryons reflect the behavior of QCD in the low-energy regime, where the QCD Lagrangian cannot be solved by a perturbative expansion. Lattice QCD calculations along with a chiral extrapolation to realistic quark masses show promise, but require further development to reach the level of detail provided by more phenomenological, approximate models such as constituent quark models (CQMs). Common to these models is the use of a confining potential in combination with a short-range residual interaction. The latter differs among the various models, the most prominent examples are one-gluon exchange [10], Goldstone boson exchange [11], and instanton-induced interactions [12]. But is there really a single short-range interaction? While there is general agreement that hadrons are built of quarks and gluons, the detailed understanding of the relevant degrees of freedom and their interactions, which determine the excitation spectrum, is still missing. Thus, knowledge of the properties of baryon resonances will shed light on the structure of non-perturbative QCD.

Although these CQMs use somewhat different approaches, they are generally quite successful in describing the masses of low-lying states. At higher energies, however, many of the predicted excited baryon states do not seem to be realized in nature. The following reasons might account for this phenomenon:

- $N\pi$ elastic scattering experiments have been the dominant source of information until very recently. If the so-called *missing* resonances do not couple to $N\pi$, they would not have been found in this process.
- Photoproduction data were mainly available only up to a mass of $1800\,\mathrm{MeV}/c^2$. The *missing* resonance problem appears in the mass region at and above this value.
- Polarization observables were measured only at GRAAL (Grenoble, France), LEGS (BNL, USA), ELSA (Bonn, Germany), and MAMI (Mainz, Germany) at low energies. However, polarization is crucial at higher energies where resonances strongly overlap. Single and double-polarization information will lead to much tighter constraints in the coupled-channel PWA, and will help to distinguish between different models.
- Many channels with more than one meson in the final state are still not explored. It is likely that many high-lying resonances do not decay directly into the ground state via single-meson emission but via a sequential decay chain. In such a chain, medium-mass states may be populated, although they exhibit only a weak photon coupling.

Even in the low-mass region, CQMs still exhibit severe problems. For example, the masses of the lowest-lying radial excitations of the nucleon or of the $\Delta(1232)$ do not match the predictions. These are the $N(1440)P_{11}$ (*Roper* resonance) (Fig. 2) and the $\Delta(1600)P_{33}$ (Fig. 1), respectively. This so-called *Roper* problem also occurs for the lowest-lying radial excitations of the Λ^* and Σ^* resonances. Another example are the negative-parity Δ states with masses around 1900 MeV/c^2. These Δ resonances, i.e. $\Delta(1900)\,S_{31}$, $\Delta(1940)\,D_{33}$ and $\Delta(1930)\,D_{35}$, are expected at significantly higher masses by constituent quark models (Fig. 1).

In addition, there are other phenomenological observations which are only poorly understood. For example, the N and Δ excitation spectrum may exhibit parity doublets, i.e. states of equal total angular momentum but with opposite parity which are almost degenerate in mass. Spin-parity partners are predicted for the known states $\Delta_{11/2^+}(2420)$, $N_{13/2^+}(2700)$,

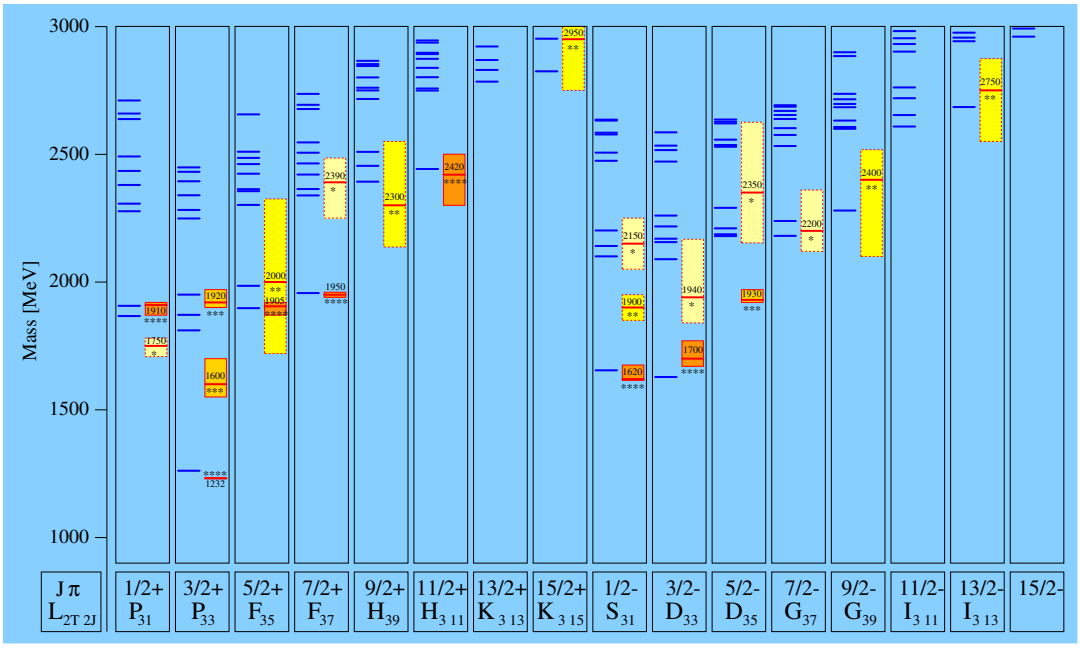

Figure 1: Δ^* *resonances using instantons as short-range interaction [12]. The left side of each column shows model predictions, whereas the corresponding right side illustrates experimental findings. The number of* $*$*'s indicates the ranking of the state according to the* **P***article* **D***ata* **G***roup (PDG) [13], i.e. a four-star state being a well established resonance.*

$\Delta_{15/2^+}(2950)$ [14]. It has also been suggested in Ref. [14] that the parity-doublet structure observed in the spectrum of highly-excited baryons may be due to effective chiral restoration in the limit of large excitation energies. If chiral symmetry is indeed restored for high-mass states, then baryons should fall into representations of $\mathrm{SU}(2)_L \times \mathrm{SU}(2)_R$ that are compatible with the given parity of the states − the parity-chiral multiplets. It is even shown that the available spectroscopic data for nonstrange baryons support the possibility of excited baryons falling into a $(1/2, 1) \oplus (1, 1/2)$ representation of the discussed symmetry [14], i.e. one parity doublet in the nucleon spectrum and one parity doublet in the Δ spectrum of the same spin being degenerate in mass. In many cases, the effect is striking: states with identical J but opposite parity often have very similar masses. This suggestion of parity doubling in the spectrum is intriguing, but the observations of masses of these states are not precise enough to make definite conclusions. For this reason, new experimental studies are certainly needed [15]. Among constituent quark models, only those based on instanton-induced forces describing the short-range interaction between quarks account naturally for this effect.

Over the last decade, indications for only a few new resonances have been reported. The analyses of the SAPHIR data on η' and hyperon photoproduction give some evidence for two new states around 1900 MeV/c^2. The $\gamma\,\mathrm{p} \;\rightarrow\; \mathrm{p}\,\eta'$ SAPHIR data propose the existence of a third S_{11} at 1890 MeV/c^2 and a P_{11} at 1980 MeV/c^2 [16]. However, it was shown that the data could also be described without an additional P_{11} [17]. Here, the S_{11} interferes with the Regge-trajectory exchanges. The $\gamma\,\mathrm{p} \rightarrow \mathrm{K}^+\Lambda$ SAPHIR data [18] indicate an additional D_{13} resonance with a mass of about 1900 MeV/c^2 [19]. New higher-statistics data on $\gamma\,\mathrm{p} \rightarrow \mathrm{K}^+\,\Lambda$, $\gamma\,\mathrm{p} \rightarrow \mathrm{K}^+\,\Sigma^0$, and $\gamma\,\mathrm{p} \rightarrow \mathrm{K}^0\,\Sigma^+$ from SAPHIR [20], CLAS [21], and LEPS [22] for center-of-mass energies between 1.6 and 2.3 GeV/c^2 indicate that more than one resonance may

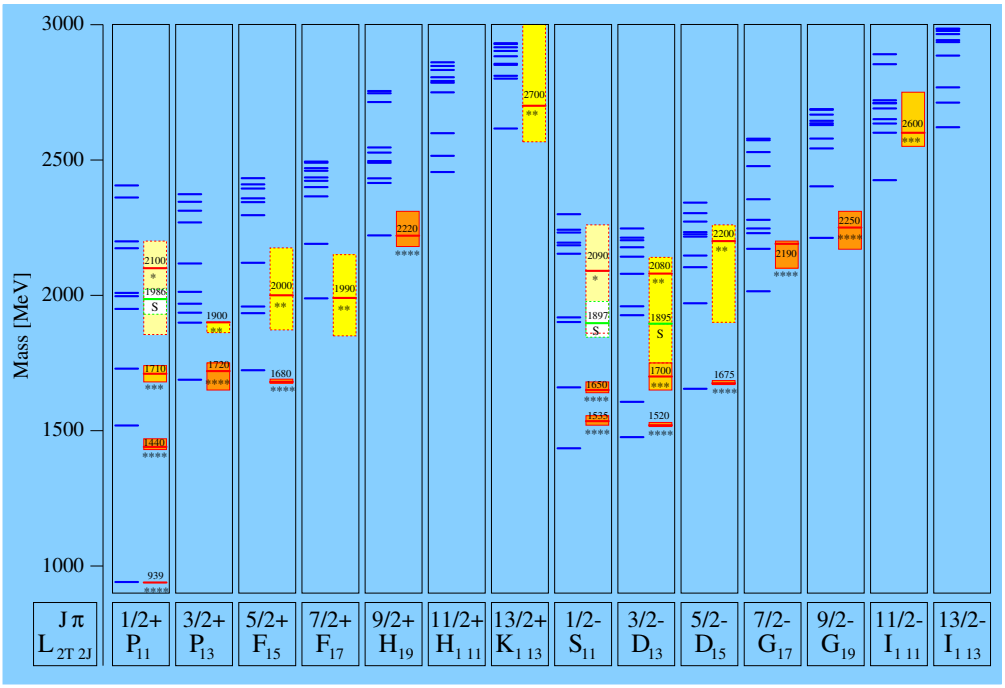

Figure 2: *N* resonances using instantons as short-range interaction [12]. The left side of each column shows model predictions, whereas the corresponding right side illustrates experimental findings. The number of ∗'s indicates the ranking of the state according to the PDG [13], i.e. a four-star state being a well established resonance.*

contribute to the mass region around 1900 MeV/c^2. A combined PWA of these data sets with additional data from a variety of other sources reveals evidence for a $P_{11}(1840)$, two D_{13} states at 1875 MeV/c^2, and optimistically, a state at 2170 MeV/c^2 [23]. In this analysis, which also included the new CB-ELSA η [24] and π^0 [25] photoproduction data, evidence for a further state, $D_{15}(2070)$, was found coupling strongly to pη.

The observation of baryon cascades (decays of high-lying states via the emission of a single π) in $\gamma\,\mathrm{p} \rightarrow \mathrm{p}\,\pi^+\,\pi^-$ at CLAS for incident photon energies above 2 GeV opens up new ways to search for missing resonances. While the proposed states $D_{13}(1875)$, $D_{15}(2070)$, and $D_{13}(2170)$ fit nicely to the quark model predictions of states, this is not true for the $P_{11}(1840)$. The possible existence of an additional P_{13} state around 1700 MeV/c^2 in CLAS electroproduction data would also contradict the quark model expectations [26].

3 Motivation

In recent years, results in baryon spectroscopy have indicated that 3-body final states are very likely to be the key for the discovery of higher-lying *missing* states because they account for most of the cross section above $W \approx 1.7$ GeV. Highly excited baryon states are predicted to decay into particles with higher masses, i.e. excited intermediate states rather than a ground-state nucleon and a meson. Calculations of decays for those resonances into two-particle channels like Nπ, Nη, and Nω yield very small partial widths. However, high-mass states have total widths of at least 150 MeV, thus the remaining decay strength must lie in reactions with higher thresholds. In the past, 2-body final states have been largely explored.

Nonetheless, many questions in the field of single-meson production are still awaiting an answer and the planned FROST program on different final states is a scientific *must*. Among other things, it is still not clear whether there is a third S_{11} resonance in η photoproduction and also the new state, $D_{15}(2070)$ [24], needs to be confirmed. These measurements are subject of the accompanying proposal E05-012 [5].

One of the key experiments in the search for missing states is the investigation of double-pion photoproduction. Quark models predict large couplings of those states to $\Delta\pi$, for instance. Such decay modes are difficult to detect since they require detectors with a large angular acceptance, and a much more involved analysis than elastic pion scattering. These ideas supported the construction of CEBAF and of the CLAS spectrometer. The investigation of high-lying states in these final states, in particular at JLab, has started only recently. The reaction $\gamma\,\mathrm{p} \rightarrow \mathrm{p}\,\pi^+\,\pi^-$ is difficult to analyze due to large non-resonant background contributions. However, it is well suited to search for states decaying into $\Delta\pi$ and $\mathrm{p}\rho$ given the high branching fractions of $\Delta \rightarrow \mathrm{N}\pi$ and $\rho \rightarrow \pi^+\pi^-$. The determination of resonance contributions based on current analyses of unpolarized data on double-pion photoproduction are ambiguous, especially at higher energies. For this reason, we propose to use the CLAS spectrometer and the newly developed frozen-spin target (FROST) at JLab in order to measure the important polarization observables for this reaction.

There is a lot of interest in $\pi^+\pi^-$ photoproduction and this will be discussed in the following sections for different energy regions. Even well known resonances have significant photoproduction amplitudes and couplings to $\mathrm{N}\pi\pi$. These states will provide *anchors* for our analyses. That is, in order to trust any identification of previously unknown states, we will be able to pick out some of the better known states and determine their unknown properties.

Low-Energy Range ($\mathbf{W \lesssim 1700}$ MeV)

The internal structure of the $P_{11}(1440)$ (*Roper* resonance) is a controversial issue. In quark models, where it is treated as an infinitely long-lived bound state, its mass is expected above the lowest-lying negative-parity state ($\rightarrow S_{11}(1535)$), but the experimentally determined mass is certainly below 1535 MeV/c^2 [12, 27]. For this reason, other interpretations have been proposed. For example, the $P_{11}(1440)$ could be a dynamically-generated resonance effect [28], or a state with a strong gluonic component [29]. In spite of intense interest in this state, the parameters of the $P_{11}(1440)$ are poorly known and depend strongly on the data and the analysis method used. Thus, the measurement of polarization observables is an important step towards an unambiguous determination of its properties.

Although the $D_{13}(1520)$ is a well established resonance, the strength of its contribution to the $\gamma\,\mathrm{p} \rightarrow \mathrm{p}\,\pi^+\,\pi^-$ cross section is still under debate. Different models lead to very different interpretations of the $\mathrm{p}\,\pi^+\,\pi^-$ data. In the Valencia model [30], the $D_{13}(1520)$ decaying into $\Delta(1232)\pi$ is the dominant contribution, whereas in the Laget model [31], the decay of the Roper resonance into $\mathrm{p}\sigma$ clearly dominates. Thus, these models are in contradiction even though they both lead to a reasonable description of the total cross section. Surprisingly, the D-wave $\Delta\pi$-decay width of the $D_{13}(1520)$ seems to be larger or at least of the same order of magnitude as the S-wave decay width. The Particle Data Group (PDG) lists $10-14\,\%$ and $5-12\,\%$ for D-wave and S-wave, respectively. This is not compatible with the naive expectation that decays involving higher angular momenta should be suppressed. In the analysis of unpolarized $\pi^+\pi^-$ CLAS data, it is difficult to fix the ratio since the value is in a range where it interferes with the contact term decaying to $\Delta\pi$ in S-wave [32].

The $P_{33}(1600)$ resonance plays a similar role in the quark model as the $P_{11}(1440)$ and is sometimes called the *Roper* of the Δ system. Both have masses much below the quark model expectations, but while different interpretations are often discussed for the $P_{11}(1440)$, not much attention has been paid to a better understanding of the $P_{33}(1600)$. The experimental uncertainty in the mass determination is considerable and a more precise knowledge of the $P_{33}(1600)$ mass would solidify this discussion. Unfortunately, the photocoupling of this state appears to be small and thus, it remains to be seen whether it will affect 2π photoproduction data.

Medium-Energy Range (1700 MeV $\lesssim$ W $\lesssim$ 1900 MeV)

In the third resonance region, the analysis of unpolarized data reveals many resonant contributions, e.g. from the $F_{15}(1680)$, $D_{13}(1700)$, $D_{33}(1700)$, and $P_{13}(1720)$. It is very difficult to decompose the cross section into the contributions from these different states without additional information from polarization observables. Most of these resonances are well established, whereas helicity couplings and their isobar contributions to the $p\,\pi^+\,\pi^-$ final state are less well known.

The CLAS Collaboration has recently reported a discrepancy between the properties of the $P_{13}(1720)$ as determined by their data and the properties listed by the PDG. The discrepancy may hint at the existence of two close-by P_{13} states. However, quark models predict only one P_{13} state in the mass region below 1900 MeV/c^2. Hence, the existence of a second resonance in this partial wave would be a surprising discovery. This question must be studied carefully.

High-Energy Range (W $\gtrsim$1900 MeV)

Quark models based on three constituent degrees of freedom predict a plethora of states above 1.8 GeV/c^2, but the number of observed states is rather limited. This is the problem of the so-called *missing* states. These states are predicted by quark models which examine both the spectrum and strong decays of resonances to couple strongly to channels like $\Delta\pi$, but not to $N\pi$. For this reason, the *missing* resonances could not have been observed in experiments using pion beams, which have provided most of the existing information on baryon resonances. Many of these *missing* states are also expected to have reasonable γp couplings and thus, should be observable in the reaction $\gamma\,p \rightarrow p\,\pi^+\,\pi^-$. It is an open question whether the states predicted by symmetric quark models really exist, or whether these models are simply not appropriate to describe the baryon spectrum. As an alternative, a quark-diquark picture of baryons can explain the reduced number of observed states. The group of positive-parity nucleon states, $P_{11}(2100)$, $P_{13}(1900)$, $F_{15}(2000)$, $F_{17}(1990)$, form an ideal way of testing this idea. These resonances form the first quartet of states which cannot be reproduced by those quark models in which one pair of quarks is frozen into a ground-state diquark. Both oscillators have to be excited and hence, they are of considerable scientific importance. On the other hand, the Particle Data Group assigns only one- and two-star ratings to these states, i.e. calling the evidence for their existence *fair*. More data are urgently needed.

The negative-parity Δ resonances around 1900 MeV/c^2 (Fig. 1) pose a problem similar to that of the $P_{11}(1440)$ and the $P_{33}(1600)$: their masses are much lower than predicted by quark models. However, only one of the observed three states is given a 3-star rating, and even the existence of this state is highly controversial. A verification of these states would pose a serious problem for quark models. Another phenomenological and poorly understood

$J = \frac{1}{2}$	$N_{1/2^+}(2100)$	$N_{1/2^-}(2090)$	$\Delta_{1/2^+}(1910)$	$\Delta_{1/2^-}(1900)$
$J = \frac{3}{2}$	$N_{3/2^+}(1900)$	$N_{3/2^-}(2080)$	$\Delta_{3/2^+}(1920)$	$\Delta_{3/2^-}(1940)$
$J = \frac{5}{2}$	$N_{5/2^+}(2000)$	$N_{5/2^-}(2220)$	$\Delta_{5/2^+}(1905)$	$\Delta_{5/2^-}(1930)$
$J = \frac{7}{2}$	$N_{7/2^+}(1990)$	$N_{7/2^-}(2190)$	$\Delta_{7/2^+}(1950)$	$\Delta_{7/2^-}(2200)$
$J = \frac{9}{2}$	$N_{9/2^+}(2220)$	$N_{9/2^-}(2250)$	$\Delta_{9/2^+}(2300)$	$\Delta_{9/2^-}(2400)$

Table 1: Parity doublets of high-lying N^* and Δ^* resonances [14].

observation is the possible existence of parity doublets, i.e. states of the same total angular momentum but with opposite parity that are almost degenerate in mass. In Ref. [14], it has been suggested that the parity-doublet structure observed in the spectrum of highly-excited baryons may be due to the restoration of an effective chiral symmetry in the limit of large excitation energies. On the other hand, quark models based on instanton-induced forces can naturally explain this effect [12]. Table 1 shows some N^* and Δ^* masses above 1.9 GeV/c^2, for states with positive and negative parity. In many cases, the effect of parity doubling is striking, indeed. For example, the first six Δ states in Table 1 with $J = 1/2,\ 3/2,\ 5/2$, and positive/negative parities are clearly degenerate. They form three parity doublets. The $\Delta_{7/2^+}(1950)$ and the $\Delta_{7/2^-}(2200)$ should also form a parity doublet, but the $\Delta_{7/2^+}(1950)$ has a mass very much closer to the other three positive-parity resonances, i.e. it does not really fit to the $\Delta_{7/2^-}(2200)$. The four positive-parity resonances rather seem to belong to a spin quartet of states with intrinsic orbital angular momentum $L = 2$ and intrinsic spin $S = 3/2$ coupling to $J = 1/2, ..., 7/2$, whereas the negative-parity states belong to a triplet with $L = 1$ and intrinsic spin $S = 3/2$. The question arises whether the parity doublets occur really due to the restoration of chiral symmetry or whether the parity doublets reflect a symmetry of the underlying quark dynamics. Only the experimental investigation of the high-mass baryon spectrum can reveal if each state really has its parity partner.

Polarization observables play an important role in order to unambiguously determine which resonances contribute, especially in the high-mass range. They will allow a determination of the helicity ratios of the resonances, and, due to their sensitivity to interference effects, they will also allow the determination of the properties of resonances, such as masses and widths, with much higher precision. The contribution of resonances coupling only weakly to the $p\,\pi^+\,\pi^-$ channel can be investigated using polarization observables. As mentioned before, a classic example of the power of polarization observables is the determination of the small η coupling of the $D_{13}(1520)$ from beam-asymmetry measurements.

3.1 Previous Measurements

A good summary of double-pion photoproduction is given in Ref. [37]. Until quite recently, data for double-pion production came mostly from bubble chamber experiments. For this reason, $\gamma\,p \rightarrow p\,\pi^+\,\pi^-$ is the only isospin channel in the so-called second resonance region ($W \approx 1500$ MeV) which has been measured with reasonable precision. Total cross sections and invariant mass distributions of the $\pi^+\pi^-$, $p\pi^+$, and $p\pi^-$ pairs are available in the literature [38, 39, 40, 41, 42, 43, 44]. During the last few years, the isospin channel with neutral particles became accessible. In a series of experiments with the DAPHNE [45] and TAPS [46, 47] detectors at the Mainz accelerator facility MAMI, all isospin channels except $\gamma\,n \rightarrow n\,\pi^+\,\pi^-$ were measured up to the second resonance region [33, 34, 48, 49, 50, 51,

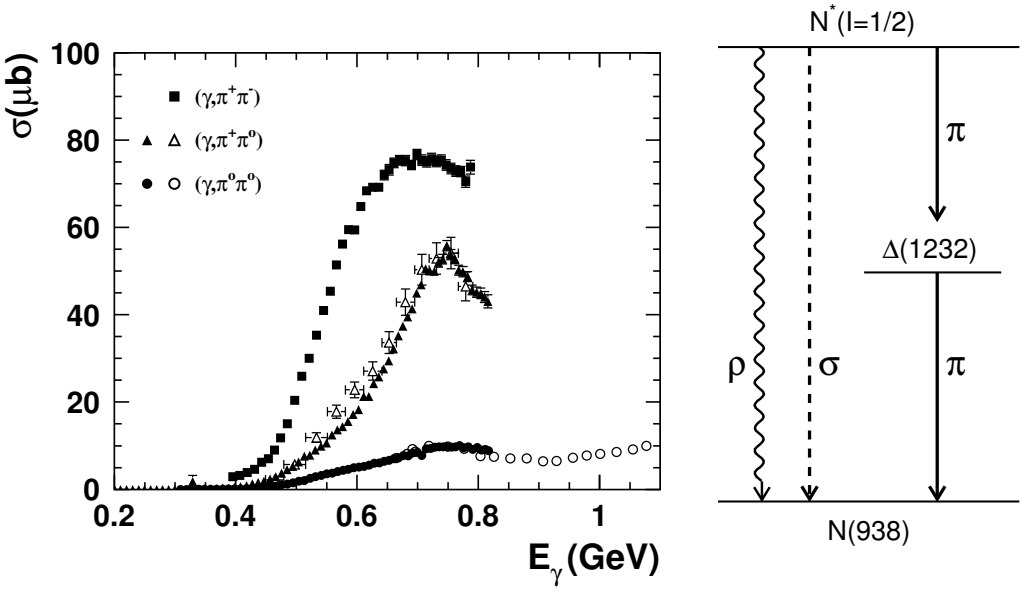

Figure 3: **Total cross sections of the 3 isospin channels of $\pi\pi$ production off the proton** *Data are from [33, 34, 35, 36]. The right hand side shows possible resonance contributions to double pion production in the second resonance region.*

52]. The two detectors are complementary in the sense that DAPHNE has advantages for reactions with many charged particles in the final state, whereas TAPS is optimized for the 2γ decay of the neutral pion. At higher incident photon energies, the $2\pi^0$ final state became available at GRAAL in Grenoble ($E_\gamma < 1.5$ GeV) [36] and the $\pi^+\pi^-$ final state at SAPHIR in Bonn [53]. Very recently, $\pi^+\pi^-$ has been studied at CLAS and $\pi^0\pi^0$ at CB-ELSA in Bonn [54] for incident photon energies up to 3 GeV.

The reaction $\gamma\,\mathrm{p} \rightarrow \mathrm{p}\,\pi^+\,\pi^-$ was analyzed in an early stage by Lüke and Söding aiming to extract the dominant production mechanisms [55]. The total cross section is small between threshold at $E_\gamma = 310$ MeV and 400 MeV. It then rises to a maximum at 650 MeV (Fig. 3). This rise reflects the $\gamma\,\mathrm{p} \rightarrow \Delta\,\pi$ threshold smeared by the width of the Δ resonance. It is accompanied by a strong peak at the mass of the Δ in the invariant mass distribution of $\mathrm{p}\pi^+$. This peak is absent in the $\mathrm{p}\pi^-$ distribution. For this reason, an important contribution is assigned to the $\gamma\,\mathrm{p} \rightarrow \Delta^{++}\,\pi^-$ channel while the $\gamma\,\mathrm{p} \rightarrow \Delta^0\,\pi^+$ is almost negligible. The $\Delta\pi$ intermediate state is likely to be populated by the decay of a resonance. However, a more detailed analysis [55] showed that the reaction is dominated by the Δ Kroll-Ruderman term and the pion pole term (Fig. 4). More recent analyses of this reaction [30, 31, 56], taking into account the new precise data from DAPHNE [33], have solidified the picture. Although there are little discrepancies between predictions and data (Fig. 4), all models find the reaction dominated by the Δ Kroll-Ruderman term. Even though the direct contribution from higher resonances is negligible in this mass region, Oset *et al.* pointed out [30] that the peak-like structure between 600 MeV and 800 MeV is due to an interference of the Kroll-Ruderman term with the sequential decay of the $\mathrm{D}_{13}(1520)$: $\gamma\mathrm{p} \rightarrow \mathrm{D}_{13} \rightarrow \Delta\pi$. This allowed the extraction of the D_{13} coupling constant to $\Delta\pi$ [57]. At higher photon energies ($E_\gamma < 2$ GeV), the invariant mass distributions of the SAPHIR data show clear signals for $\Delta \rightarrow \mathrm{N}\pi$ and $\rho \rightarrow \pi^+\pi^-$ contributions [53].

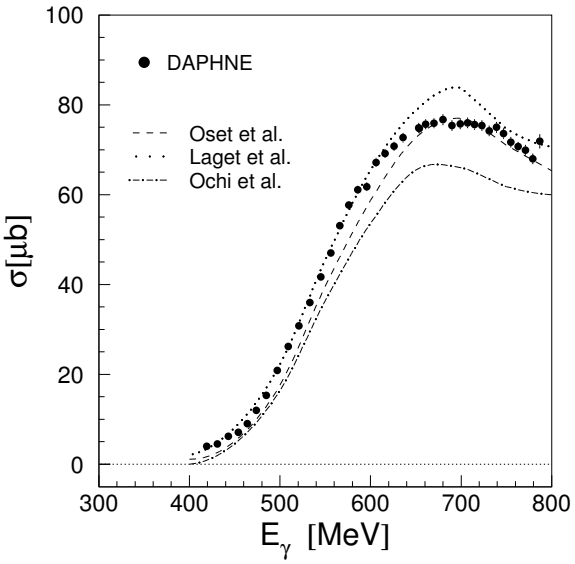

Figure 4: **Data on $\gamma\,\mathbf{p} \rightarrow \mathbf{p}\,\pi^+\,\pi^-$**
Total cross section for the reaction $\mathrm{p}\gamma \rightarrow \mathrm{p}\pi^+\pi^-$. *Data are from [33]. Dashed, dotted, and dash-dotted curves represent calculations [30, 31, 56].*

At CLAS, the isobar model for a phenomenological analysis of double-charged pion production induced by real and virtual photons in the entire N* excitation region was developed in collaboration between Jefferson Lab and Moscow State University (MSU). This approach relates the N* photocouplings and hadronic parameters to measured integrated, single and multi-differential cross sections for the $\mathrm{p}\,\pi^+\,\pi^-$ final state, allowing to extract N* photocouplings and, in part, hadronic decay parameters from a fit to the data. In the 2003-JLab-MSU model, the contributions from the isobar channels $\Delta^{++}\pi^-$, $\Delta^0\pi^+$, $\mathrm{p}\rho$, and $\mathrm{D}_{13}(1520)\pi^+$ were taken into account. The remaining mechanisms of the unknown dynamics were parametrized as 3-body phase space with the amplitude dependent on the photon energy and virtuality only [26, 58, 59]. A combined analysis of recent CLAS photo- and electroproduction data [60] allowed a considerable improvement of this approach. For the first time, the contributions from the isobar channels $\mathrm{F}_{15}(1685)\pi^+$, $\mathrm{P}_{33}(1600)\pi^-$, as well as direct 2π production mechanisms were observed. The quality of the CLAS data allowed determination of all relevant mechanisms in 2π photo- and electroproduction from the data fit without any need for remaining mechanisms of unknown dynamics. A good description of all available CLAS/world unpolarized observables in double-charged pion channels was achieved in the entire N* excitation region. The reliability of the background treatment and N*/background separation was confirmed in a combined analysis of CLAS π and 2π electroproduction data [61]. Data on the Q^2 evolution of the N* photocouplings for most excited proton states in the mass range between $1.4 - 2.0$ GeV/c^2 were extracted in the analysis of CLAS experiments within the framework of the 2005-JLab-MSU isobar model and for the first time for many high-lying nucleon excitations with masses above 1.6 GeV/c^2.

Most background terms are excluded in the $\pi^0\pi^0$ final state since the photon does not couple to the neutral pion and the ρ meson does not decay into a pair of neutral pions. The total cross section was measured by TAPS in the low-energy regime [48, 51] and by GRAAL up to an incoming photon energy of $E_\gamma = 1.5$ GeV [62]. Two peak-like structures are observed [48, 51, 62] and have been interpreted within the Laget model [31, 62] and the Valencia model [30]. In the Valencia model for the low-energy region, the $\mathrm{D}_{13}(1520)$ decaying into $\Delta(1232)\pi$ is the dominant contribution whereas in the Laget model, the decay of the *Roper* resonance ($\mathrm{P}_{11}(1440)$) decaying into $\mathrm{p}\sigma$ is clearly dominating. Thus, both models are in

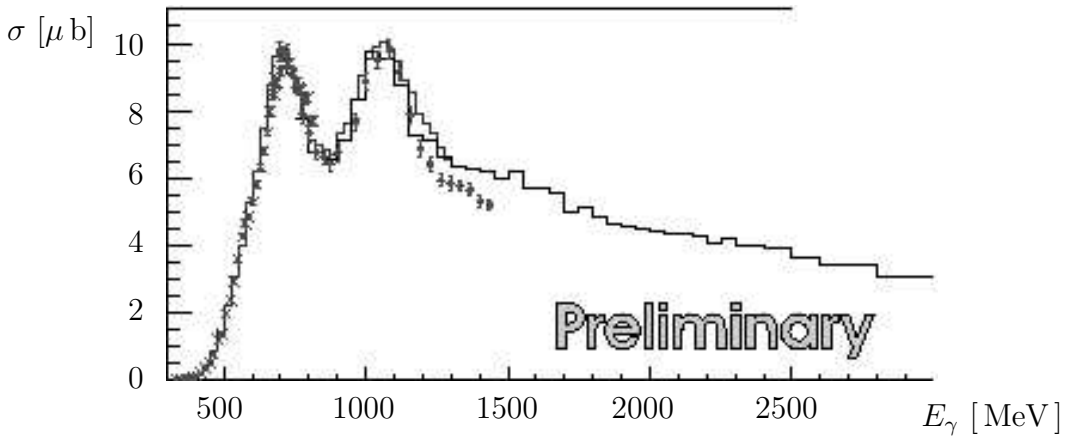

Figure 5: **Total cross section for the reaction $\gamma\,\mathrm{p} \rightarrow \mathrm{p}\,\pi^0\,\pi^0$**
Total cross section obtained by integrating the result of the partial wave analysis over phase space (solid line) in comparison to the preliminary TAPS (x) and GRAAL (∘) data.

contradiction even though they lead to a reasonable description of the total cross section. CB-ELSA has taken data on $\gamma\,\mathrm{p} \rightarrow \mathrm{p}\,\pi^0\,\pi^0$ extending the covered energy range to $E_\gamma = 3$ GeV. First results of an event-based PWA have been shown at international conferences. The PWA technique used at ELSA is the covariant tensor formalism [63] which will also be presented later in this proposal. The fits include preliminary TAPS data in the low-energy region in addition to CB-ELSA data. Resonances with different quantum numbers are introduced in various decay modes, i.e. $\Delta(1232)\pi$, $\mathrm{N}(\pi\pi)_\mathrm{S}$, $\mathrm{P}_{11}(1440)\pi$, $\mathrm{D}_{13}(1520)\pi$ and $\mathrm{X}(1660)\pi$. For a good description of the data, the $\mathrm{P}_{11}(1440)$, $\mathrm{D}_{13}(1520)$, $\mathrm{D}_{13}/\mathrm{D}_{33}(1700)$, $\mathrm{P}_{13}(1720)$, $\mathrm{F}_{15}(1680)$ resonances are clearly needed. A preliminary result is a strong contribution of the $\mathrm{D}_{13}(1520) \rightarrow \Delta\pi$ amplitude in the region of the first peak-like structure in the total cross section [54]. The total cross sections measured by the DAPHNE and TAPS detectors at Mainz also agree better with the result of the Valencia model in spite of a systematic discrepancy between the DAPHNE and the TAPS data.

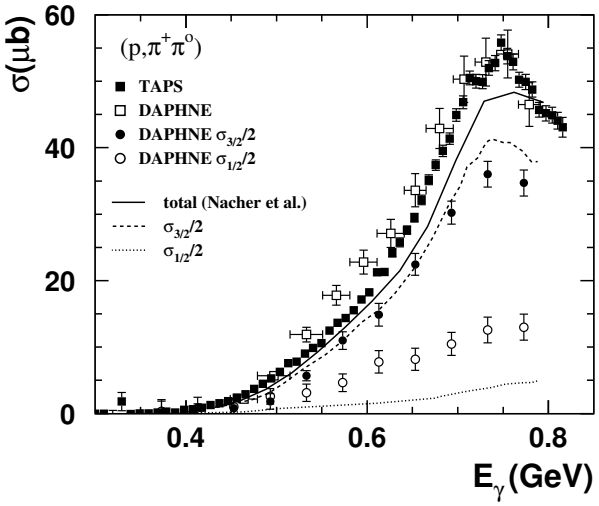

Figure 6: **Helicity dependence**
Helicity dependence of the reaction $\gamma\,p \rightarrow n\,\pi^0\,\pi^+$. Shown are the total cross section and the $\sigma_{\frac{3}{2}}$ and $\sigma_{\frac{1}{2}}$ partial cross sections. Data are from [34, 49, 64]. Model predictions are from Nacher et al. [65, 66]

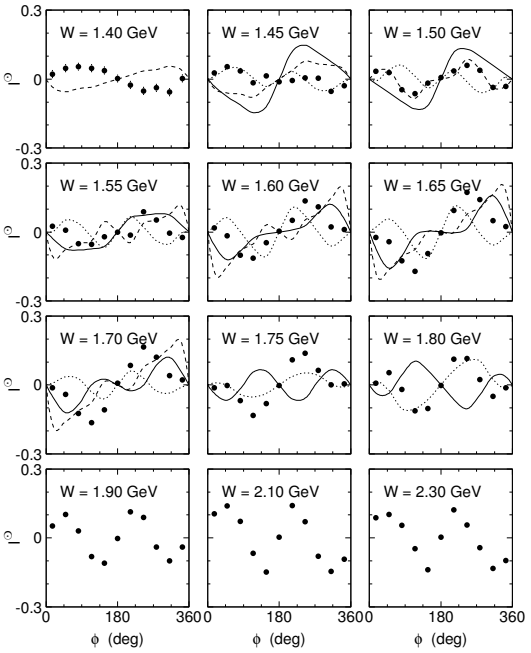

Figure 7: **Asymmetry $I^{\odot}$ in $\vec{\gamma}\,p \to p\,\pi^+\,\pi^-$ [67]** *Angular distributions for selected center-of-mass energy bins (ΔW = 50 MeV) of the cross-section asymmetry. The data are integrated over the detector acceptance. The statistical uncertainties are mostly smaller than the symbol size. The solid and dotted curves are the results from model calculations by Mokeev et al. [26, 68, 59] (for 1.45 GeV $\leq$ W $\leq$ 1.80 GeV) with relative phases of 0 and π between the background and $\Delta\pi$-subchannel amplitudes, respectively. The dashed curves show results of calculations by Fix and Arenhövel [69] (for W $\leq$ 1.7 GeV). ϕ is defined as the π^+ azimuthal angle in the rest frame of the $\pi^+\pi^-$ system with the z direction along the total momentum of the $\pi^+\pi^-$ system (helicity frame).*

Invariant mass distributions clarified the relative importance of the different reaction mechanisms in the second resonance region involving resonance decays (sequential decay with an intermediate $\Delta\pi$ state, emission of a ρ meson, etc.). However, it is difficult to assign these reaction mechanisms to a specific resonance. For example, the large importance of the D_{13} and the negligible contribution of the S_{11} in the models result from photon couplings and the decay widths which are input parameters for the calculations. However, the GDH collaboration has recently measured the helicity dependence of the cross section for the $n\pi^0\pi^+$ final state [64]. The result shows that most of the resonance structure occurs in the helicity $\sigma = \frac{3}{2}$ channel (Fig. 6). A S_{11} contribution would show up in the $\sigma = \frac{1}{2}$ channel which has a flatter energy dependence and contributes less than 30 % to the total cross section. The model prediction by Nacher et al. [66] agree qualitatively with the distribution of strength on helicity 3/2 and 1/2 while underestimating the $\sigma = \frac{1}{2}$ contribution.

At Jefferson Lab Hall-B, results on two-pion photoproduction have been recently obtained in the reaction $\vec{\gamma}p \to p\pi^+\pi^-$ using a circularly-polarized tagged photon beam and an unpolarized target in the energy range between 0.6 GeV and 2.3 GeV. Cross section asymmetries are shown in Fig. 7 exhibiting strong sensitivity to the kinematics of the reaction. The data are compared with results of available phenomenological models. In the approach by Mokeev *et al.* (solid curves), double-charged pion photo- and electroproduction are described by a set of quasi-two-body mechanisms with unstable particles in the intermediate states: $\Delta\pi$, $N\rho$, $N(1520)\rho$, $N(1680)\rho$, $\Delta(1600)\pi$, and with subsequent decays to the $p\pi^+\pi^-$ final state [26, 59, 68]. Residual direct $p\pi^+\pi^-$ mechanisms are parametrized by exchange diagrams [59]. All well established resonances with observed double-pion decays are included, plus $\Delta(1600)$, N(1700), N(1710), and a new state, N(1720) with $J^P = 3/2^+$, possibly observed in CLAS double-pion data [60]. The calculations within the framework of the JLab-MSU isobar model show a huge sensitivity of the photon-beam asymmetry to the relative phases between various contributing mechanisms. As shown in Fig. 7, the variation of the relative phase between the N^*/background in the $\Delta\pi$ isobar channels in a range between 0 and 2π eventually leads to a reasonable agreement with the measured asymmetries. High

sensitivity to interference effects was predicted also for 2π electroproduction [70]. Therefore, the combined analysis of polarization observables and unpolarized cross sections will enable us to access the interference pattern between various mechanisms in 2π photoproduction. This is essential new information since in the analysis of unpolarized cross sections only, the relative phases between various mechanisms may be absorbed into phenomenological coupling constants. Instead, polarization observables are sensitive both to the magnitudes and phases between contributing amplitudes. The combined analysis of unpolarized cross sections and polarization observables in 2π channels will become particularly important in order to disentangle the $A_{1/2}$ and $A_{3/2}$ N^* photocouplings. Moreover, such analysis may provide hints on new so-called *missing* baryon states with considerably different magnitudes of $A_{1/2}$ and $A_{3/2}$ N^* photocouplings [71].

Results obtained by Fix and Arenhövel are also included in Fig. 7 (dashed curves). They use an effective Lagrangian approach with Born and resonance diagrams at the tree level [69]. The model includes the nucleon, the $\Delta(1232)$, N(1440), N(1520), N(1535), N(1680), $\Delta(1620)$, N(1675), and N(1820) resonances, as well as the σ and ρ mesons. Neither of the models is able to provide a reasonable description of the beam-asymmetry data over the entire kinematic range covered in the experiment. This is an indication of the particular sensitivity of the beam asymmetry to interference effects among various amplitudes.

In summary, a better understanding of the experimental spectrum is certainly needed. Although a large amount of unpolarized cross section measurements of double-pion photo- and electroproduction on the proton have been reported by several collaborations, the database collected for polarization observables remains quite sparse. The latter will provide additional constraints for models and partial wave analyses (PWA). This also increases the sensitivity on smaller contributions and will help to distinguish between ambiguous PWA solutions. It has to be pointed out that all published results on double-pion photoproduction are based on invariant mass distributions and cross sections. Event-based analyses are still in a preliminary stage. However, the latter approach is very important because it takes all correlations of 5 independent variables properly into account.

3.2 Theoretical Predictions

On the theoretical side, some experience has been gained during the last decade [30, 65, 66, 26, 68, 59, 69, 72, 73]. It should be noted that the various models which are presently used are constructed according to the same scheme: effective Lagrangian densities, where the parameters for resonant and background mechanisms are either taken from other experiments or are treated as free parameters in the analysis. Aside from the wide variations in the corresponding coupling constants allowed by the PDG [74], the primary source of differences between the models is the treatment of the background, which appears to be very complicated in the effective Lagrangian approach for double-pion photoproduction. A better understanding of the double-pion photoproduction dynamics is vital for the reliable extraction of N^* photocouplings.

The constituent quark model of Capstick and Roberts [75] predicts many excited baryon states in the range of photon energies available at Jefferson Lab. In Table 6 in appendix A, the decay amplitudes for the lightest few negative-parity nucleon resonances into various channels based on their model are listed. It has to be pointed out that this table represents only a list of a few resonances out of the many predicted excited baryon states. On the average, the *missing* resonances around 2 GeV/c^2 and above show only weak couplings to channels like Nπ, Nη and Nη'. However, these states exhibit large branching fractions to

	$N\pi$	$N\eta$	$N\eta'$	$N\omega$	$\Delta\pi$	$N\rho$
$S_{11}(1945)$	32	6	13	32	45	**330**
$S_{11}(2030)$	14	1	2	8	32	1
$S_{11}(2070)$	4	<1	1	42	**170**	60
$S_{11}(2145)$	<1	<1	<1	<1	1	5
$S_{11}(2195)$	<1	<1	<1	<1	4	10

Table 2: **Partial widths of S_{11} resonances.** *Masses and partial widths are taken from [75], see also Table 6 in appendix A. Errors are suppressed for reasons of clarity.*

$\Delta\pi$ and $N\rho$. For this reason, they should be observable in these final states. The level of agreement between the calculations and the available widths from the partial wave analyses is encouraging, indeed.

We exemplify the need for precise data on various final states by discussing one particular resonance, i.e. $S_{11}(2090)$ of the Particle Listing [13]. The resonance was first found by Höhler [76] and collaborators and confirmed by Cutkosky et al. [77] in elastic $N\pi$ scattering data. Manley and others [78] included bubble chamber data on $\pi^+\pi^-$ production and found possible evidence for the $N\rho$ as well as the $\Delta\pi$ decay mode of the resonance. The PDG assigns a mass of 2090 MeV (and an essentially undefined width) and omits the resonance completely from the summary table. The decay modes are also more suggestive than established. The SAPHIR Collaboration confirmed the strong rise at threshold of the η' photoproduction cross section [16] for which indications had been found earlier. The statistics of ≈ 250 events was sufficient to determine also the differential cross sections. The SAPHIR Collaboration suggested an interpretation of the data as by two resonances, i.e. $S_{11}(1890)$ and $P_{11}(1980)$, as discussed in the previous section.

In Ref. [75, 79], the mass spectrum and the decay widths of a large number of resonances were calculated. In the region of the $S_{11}(1890)$ discussed above, five states with different masses and different decay patterns occur. Table 2 reproduces part of their results for the partial widths. It seems to be very difficult to establish 5 different states in such a small mass intervall. However, if the states do exist, their mass observed in $N\rho$ and $\Delta\pi$ must differ by more than 100 MeV. Therefore, the comparison of the mass spectra of photoproduced ρ mesons and of the $\Delta\pi$ system will give a strong indication if more than one state is produced. Other examples can be derived from the tables in [75].

4 Proposed Experimental Configuration

4.1 Tagged-Photon Beams

The field of photo-induced reactions is generally approached by two different techniques of creating a tagged-photon beam. At SPring-8 ($E_\gamma < 2700$ MeV) and GRAAL ($E_\gamma < 1700$ MeV), high-energy photons are created by Compton backscattering of laser light off an electron beam. The polarization of the laser beam is transferred to the backscattered photon beam, however in practice, the luminosity is very limited by the interaction of the high-power laser with the circulating electron beam. At ELSA ($E_\gamma < 3200$ MeV) and JLab ($E_\gamma < 6000$ MeV) on the other hand, energy-tagged photons are created using coherent bremsstrahlung. In the latter case, creation of a polarized photon beam requires more effort, but the better luminosity is a big advantage.

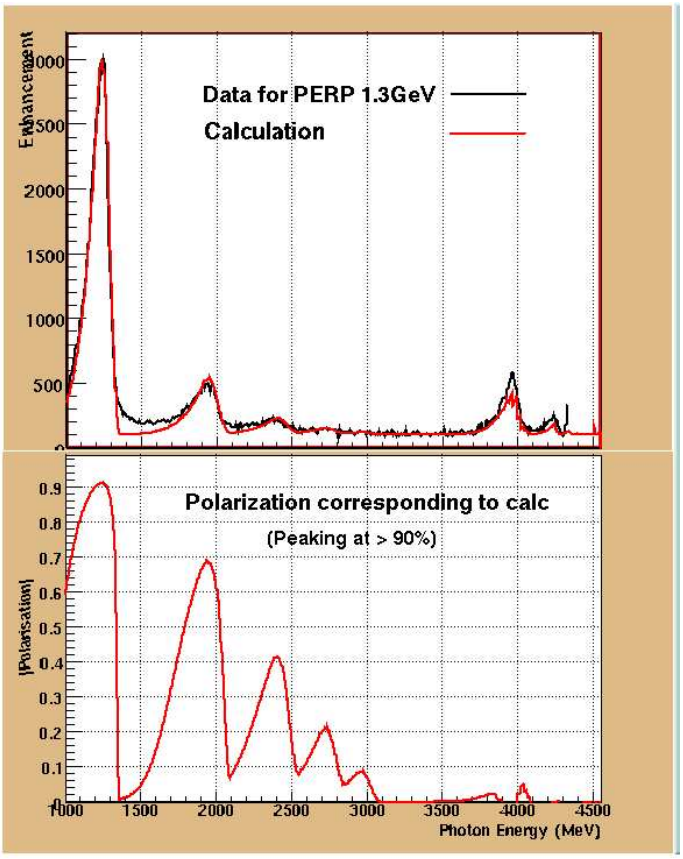

Figure 8: **Example of a linearly-polarized tagged photon spectrum obtained in Hall B (CLAS-g8)** *Over 80 % of the photon flux is confined to a 200-MeV wide energy interval. The top plot shows the photon spectrum, whereas the bottom plot shows the corresponding degree of polarization according to calculations. The dominant coherent peak is at* $E_\gamma = 1300$ *MeV and the degree of polarization is greater than 90 %. One characteristic angle is* $m_e c^2/E_0 = 0.511/4550$. *The collimator subtends two fifths of a char. angle and thus, the beam is very tightly collimated.*

Linearly-Polarized Photons

The broad-range tagging facility in Hall-B [80] has reliably provided all kinds of tagged-photon beams. Linearly-polarized photons are produced using coherent bremsstrahlung from a thin, well oriented diamond radiator. This technique was successfully employed during the CLAS-g8a and CLAS-g8b run periods. While the photon tagger generally covers a range in photon energies from 20 % to 95 % of the incoming electron beam energy, over 80 % of the linearly-polarized photon flux is confined to a 200-MeV wide energy interval. The degree of polarization can reach 80 % to 90 %. It is a function of the fractional photon beam energy and collimation. For example, production on a diamond with a thickness of 20 μm yields 70 % at $k = E_\gamma \,/\, E_{e^-} = 0.5$ and a collimation of one characteristic angle ($\theta_{\rm char} = m_e c^2/E_0$). The degree of polarization increases with lower fractional energy, e.g. to 93 % at $k = 0.3$ and the same collimation. The polarization of the collimated beam is fairly constant over a 200 MeV energy range near the coherent edge. A spectrum of linearly-polarized photons obtained in Hall-B is shown in Fig. 8.

Circularly-Polarized Photons

Circularly-polarized photon beams are produced using a beam of polarized electrons incident on the bremsstrahlung radiator. The degree of circular polarization depends on the ratio $k = E_\gamma \,/\, E_{e^-}$. It ranges from 60 % to 99 % of the incident electron beam polarization P_{e^-} for photon energies between 50 % and 95 % of the incident electron energy. The degree of polarization versus k is shown in Fig. 9. It can be determined considering the loss of electron

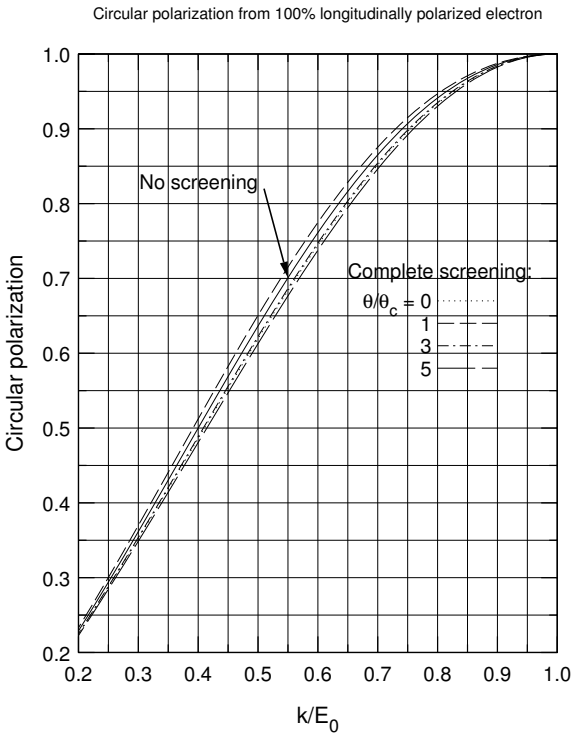

Figure 9: **Helicity transfer $\mathbf{P}_\odot$ / $\mathbf{P}_\mathrm{e}$ from the electron to the photon.**

polarization while the beam is extracted onto the radiator target and the helicity transfer from the electron to the photon. The polarisation is approximately given given by Ref. [81]:

$$P_\odot = P_\mathrm{e} \cdot \frac{4k - k^2}{4 - 4k + 3k^2} \tag{1}$$

4.2 Frozen-Spin Target

The target for use with the CLAS spectrometer is capable of being polarized transversely and longitudinally with a minimum amount of material in the path of outgoing particles. This essential piece of hardware will be used together with other approved experiments: E02-112 [2], E03-105 [3], E04-102 [4], and E05-012 [5]. The existing Hall-B polarized target is a dynamically polarized target and was used in previous electron beam experiments. It was longitudinally polarized with a pair of 5 T Helmholtz coils. The magnet needed to produce this field occupied a large fraction of the space around the target sample limiting the available aperture to 55 degrees in forward direction. For photon-beam experiments and the goal of a high-quality data sample for partial wave analysis, a frozen-spin target is a much more attractive choice.

The proposed polarized target will be positioned in the geometrical center of the CLAS spectrometer. The target cryostat will be of horizontal type with a pipe of about 200 cm in length and 25 cm in diameter used to position the target at the center of CLAS as shown in Fig. 10. Since the CLAS spectrometer is a magnetic spectrometer, its operational characteristics are very sensitive to the additional magnetic field produced by the target. For this reason, the target material will be dynamically polarized by microwave irradiation in a strong magnetic field of 5 T at a temperature of 1 K outside of CLAS. After maximum polarization is reached, the cryostat will be turned to *holding* mode (or *frozen-spin* mode)

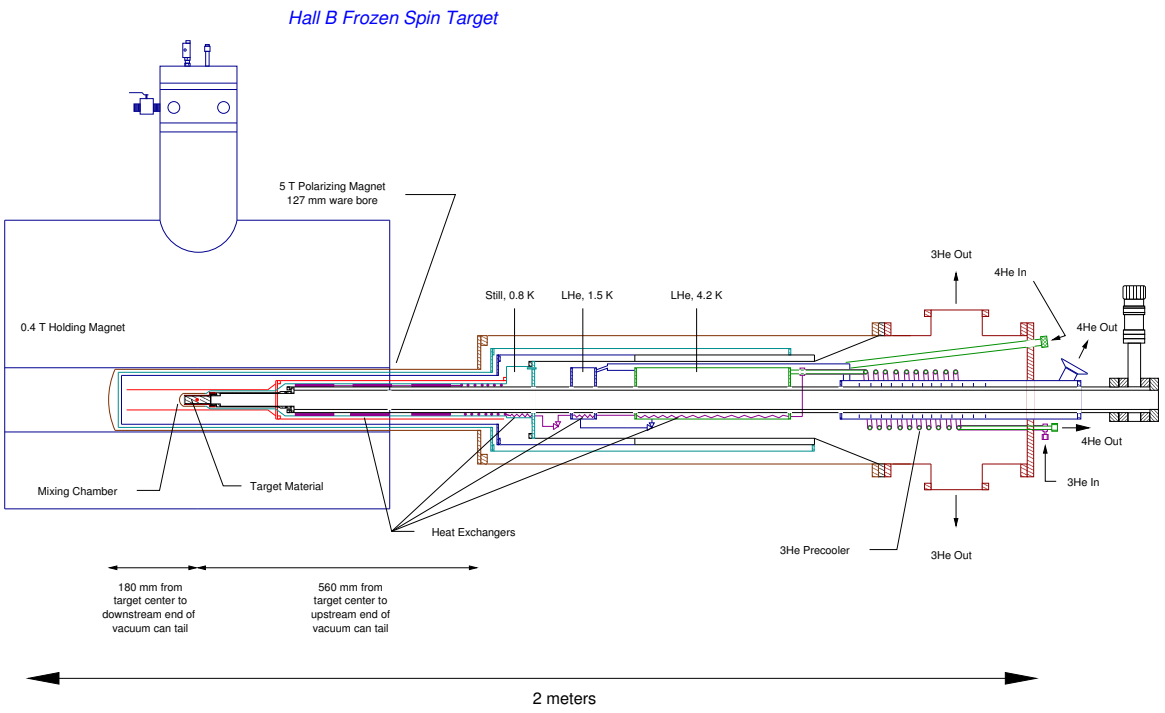

Figure 10: **Schematics of the Hall B frozen-spin target (FROST)**

with a much lower magnetic field of 0.5 T at a temperature of 50 mK and moved back into CLAS. For a butanol target, the proton polarization of initially about 90 % decreases slowly with a relaxation time of typically several days under the conditions outlined above. This is sufficiently long for a useful polarized-target experiment. Repolarization requires putting the target back into the high field. This procedure takes *only* a few hours.

The target cell will be 50 mm long and 15 mm in diameter. The length is a compromise between conflicting demands for count rate and cooling requirements. The planned target material is butanol with a dilution factor (fraction of polarizable nucleons) of approximately 13.5 %. The properties are summarized in Table 3. Such targets have been constructed with maximum polarizations of 85 % to 95 %. The design is similar to the one used at the

Chemical structure	C_4H_9OH
Dilution factor	10/74
Length	50 mm
Diameter	15 mm
Density	0.985 g/cm^3
Packing factor	0.62 ± 0.04
Effective density	0.611 g/cm^3
Longitudinal polarization (average)	0.80
Transverse polarization (average)	0.80

Table 3: **Target properties for the Frozen-Spin Butanol Target**

photonuclear facilities in Mainz and Bonn, Germany [82, 83]. The construction of the Hall-B frozen-spin target is based on experience of the JLab target group. The target is planned to be ready for operation by summer 2006.

Polarizing Magnet

A horizontal 5 T superconducting polarizing magnet with a 130 mm warm bore has been purchased from Cryomagnetics, Inc. which operates very reliably. A precise NMR measurement of its field map was performed when the magnet arrived at JLab. The details of these measurements are described in Ref. [84]. They confirm that the homogeneity of the magnetic field within the target volume (15 mm in diameter and 50 mm in length) is better than 40 ppm.

Dilution Refrigerator

For the cylindrical target volume in question, approximately 20 mW of microwave power will be necessary for the polarization process at 0.5 K considering a polarization build-up time of about 30 minutes. Under experimental run consitions the heat load from the photon beam is about 1 μW. This implies that in *frozen-spin* mode at 0.5 T and 50 mK, the refrigerator should provide a cooling power of a few μW. The only technique that satisfies these conditions is a ^{3}He/^{4}He dilution refrigerator. The latter is currently under design and construction by the JLab Target Group.

Holding Magnet

The internal holding system should be as *transparent* as possible to outgoing particles. This demands limiting the amount of conductor, which results in a holding field of lower intensity. By contrast, the relaxation time of polarization is a strong function of the magnetic field intensity, i.e. a higher field maintains the polarization longer. A holding field of about 0.5 T is currently considered. The homogeneity of the holding field within the target cell volume must be better than 1 % in order to be able to monitor the degree of polarization during run conditions.

The low holding field can be supplied either by the fringe field of the polarizing magnet or by another magnet, the geometry of which can be tailored to the particular experiment to provide a much larger acceptance than obtainable with a high-field magnet. The polarized target for the Mainz-Bonn GDH experiments [82, 83] used a longitudinal holding field produced by a very thin (500 μm) superconducting solenoid located within the target cryostat which offered virtually no obstruction to the outgoing particles. This experiment demands both longitudinal and transverse target polarizations. For this reason, two different holding magnets are needed. Extensive simulations have been performed in order to find the optimal design for a holding magnet system. Details of the study using the Poisson/Superfish-2D [85] package and the Opera-3D [86] package can be found in [87].

As a result of the simulations, a solenoid will be used for the longitudinal holding field. The simulations show that a design with three layers of NbTi superconducting wire (0.112 mm in diameter) can provide a central field intensity of up to 0.5 T with the homogeneity over the entire target cell better than 0.5 %. This will indeed allow us to monitor the target polarization via NMR. Tests of a prototype coil yielded results that confirm the simulation. For the transverse holding magnet, we are planning to use a dipole magnet with race-track

shaped coils wrapped around the cylinder. The coils will be positioned as much as possible within the shadows of the CLAS torus to minimize the loss of acceptance. The simulation shows that we can expect a field homogeneity better than 0.8 % with three or four layers of superconducting wire.

In order to determine the effective dilution factor $D_{\rm eff}$, we propose to collect data simultaneously at $10-20$ % event rate on unpolarized material by placing a carbon target ($\rho = 2.26$ g/cm^3) of 8.3 mm in length at a slightly downstream position. Additionally, we propose to take data on an unpolarized sample during the times needed to re-polarize the target.

4.3 CLAS Configuration

We will use the CLAS spectrometer in its standard configuration for the photon beam running. The frozen-spin target will be placed in the center of CLAS, and surrounded with the new start counter. We will run with the torus magnetic field set to one-half of the maximum field, outbending positive particles. For the proposed experiment, the *ideal* trigger would require the detection of at least two charged particles. This is in agreement with the experiment E02-112 [2] which has 20 days approved for measurements with linearly-polarized beam and transversely-polarized target. For the other polarization configurations, we propose to use a trigger requiring at least one charged particle in CLAS. This trigger configuration is compatible with all other approved experiments using the frozen-spin target.

CLAS is divided into six sectors by a superconducting, toroidal magnet. Immediately surrounding the target is the start counter, a set of 24 scintillators in six sectors. Their purpose is to provide a time for the start of a reaction. This time can then be matched to a *tagged* photon. From inside to outside, another set of scintillators follows the drift chambers. The scintillators or time-of-flight walls provide timing information for charged tracks used to measure velocities and energies in conjunction with the start counter. Finally, calorimeters are located in the forward region, primary used to detect neutrons and other neutral particles.

5 Analysis Techniques

Polarization observables have been used until very recently only at GRAAL, LEGS and MAMI at low energies. However, these observables are very important to disentangle different resonances, especially at higher masses where resonances strongly overlap. A major obstacle in the determination of the couplings of baryon resonances in $\pi\pi$ are the considerable contributions from non-resonant mechanism. The background dominates double-charged pion photoproduction at the level of $60-90$ % in the total cross section. Thus, polarization observables, which are sensitive to those small resonant contributions will be very helpful in the evaluation of N* parameters.

Differential cross section data, though helpful, provide little information about these small couplings. However, resonances should reveal themselves more clearly through the interference with dominant amplitudes. These interference terms can be isolated via polarization observables. A typical example for such an effect is the $D_{13}(1520)$ resonance revealing itself in the beam-asymmetry data of η photoproduction, due to its interference with the dominant $S_{11}(1535)$. The formalism and terminology for the various polarization observables of interest in double-meson photoproduction can be found in Ref. [88]. For single-meson production, the differential cross section using polarized photons (δ_l for linearly-polarized photons and $\delta_\odot$

for circularly-polarized photons) and a polarized target (Λ_x, Λ_y for transversal polarization in the reaction plane and Λ_z for longitudinal polarization) is given by:

$$\begin{aligned}\frac{\mathrm{d}\,\sigma}{\mathrm{d}\,\Omega} = \sigma_0 \{\, 1 &- \delta_l\, \mathbf{\Sigma} \cos 2\phi \\ &+ \Lambda_x\, (\, -\delta_l\, \mathbf{H} \sin 2\phi \,+\, \delta_\odot\, \mathbf{F}\,) \\ &- \Lambda_y\, (\, -\mathbf{T} \,+\, \delta_l\, \mathbf{P} \cos 2\phi) \\ &- \Lambda_z\, (\, -\delta_l\, \mathbf{G} \sin 2\phi \,+\, \delta_\odot\, \mathbf{E})\} \;.\end{aligned} \tag{2}$$

In the interesting case of two-meson or even multi-meson final states, there are more than the 7 functions **Σ, H, F, T, P, G**, and **E** observed in single-meson photoproduction, because many more kinematic variables are required in order to describe the system. For $\gamma\,\mathrm{p} \rightarrow \mathrm{p}\pi\pi$ without measuring the polarization of the recoiling nucleon, the reaction rate I can be written as [88]:

$$\begin{aligned} I \;=\; I_0 \{\, (\, 1 \,+\, \vec{\Lambda}_i \cdot \vec{\mathbf{P}}\,) \\ &+ \delta_\odot\, (\mathbf{I}^\odot \,+\, \vec{\Lambda}_i \cdot \vec{\mathbf{P}}^{\,\odot}\,) \\ &+ \delta_l\, [\, \sin 2\beta\, (\, \mathbf{I}^{\mathbf{s}} \,+\, \vec{\Lambda}_i \cdot \vec{\mathbf{P}}^{\,\mathbf{s}}\,) \\ &\qquad \cos 2\beta\, (\, \mathbf{I}^{\mathbf{c}} \,+\, \vec{\Lambda}_i \cdot \vec{\mathbf{P}}^{\,\mathbf{c}}\,)\,]\,\} \;, \end{aligned} \tag{3}$$

where $\vec{\mathbf{P}}$ represents the polarization asymmetry that arises if the target nucleon is polarized and $\vec{\Lambda}_i$ denotes the polarization of the initial nucleon. Here $\delta_\odot$ is the degree of circular polarization in the photon beam, while δ_l is the degree of linear polarization, with the direction of polarization being at an angle β to the x-axis. A *complete* set of experiments will require measurement of single, double and triple polarization observables, in addition to the differential cross sections. For processes with a hyperon in the final state, such as $\gamma\,\mathrm{N} \rightarrow \pi\,\mathrm{K}\,\Lambda$, the self-analyzing decay of the hyperon allows its polarization to be determined [2]. The polarization observables that arise for $\gamma\,\mathrm{p} \rightarrow \mathrm{p}\,\pi\pi$ are given in Table 8 in appendix B.

In case of single-pion photoproduction, the whole reaction can always be put into a single plane defined by the recoil nucleon, along with the initial photon and the target nucleon (in the center-of-mass frame). In case of two-pion photoproduction, this only happens in very special cases. However, in those special cases, Equation 2 is still valid. All observables that

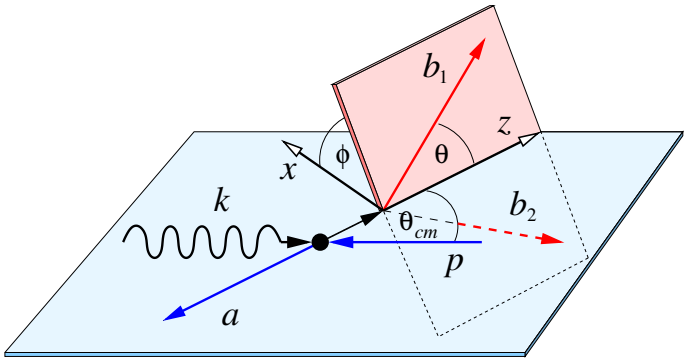

Figure 11: **Decay angles in a 3-particle final state:** *ϕ indicates the angle between the production plane and the plane formed by two of the final-state particles.*

are odd under $\phi_1 \leftrightarrow 2\pi - \phi_1$ vanish *in plane* and thus, Equation 3 reduces to Equation 2, where one possible way to define ϕ_1 is to use the π^+ azimuthal angle in the rest frame of the $\pi^+\pi^-$ system (Fig. 11). For this reason, asymmetries in double-meson photoproduction will also occur if only the beam is circularly polarized or only the target is longitudinally polarized. The differential cross section for reactions with two mesons in the final state is 5-fold differential, as is every term on the right-hand side of Equation 3. To get a 2-fold differential cross section, both sides of Equation 3 have to be integrated and divided by I_0. The asymmetries are ultimately ratios of differential cross sections.

Differential cross sections for unpolarized data on $\gamma\,\mathrm{p} \rightarrow \mathrm{p}\,\pi^+\,\pi^-$ have been published for the first time only recently [89]. However, presented in whatever form, they will only provide information on the magnitudes of helicity or transversity amplitudes. Phase information is crucial, and this is only available from measurements of a number of different observables. This is well known for processes like $\gamma\mathrm{N} \rightarrow \mathrm{N}\pi$. The same is true, or perhaps, even more true, for processes like $\gamma\mathrm{N} \rightarrow \mathrm{N}\pi\pi$ because of the number of intermediate states which can contribute to the same final state, leading to a large number of parameters to be determined. Models with quite different input can and will succeed in describing the total and differential cross section, but the polarization observables will serve to distinguish among such models. The photon polarization asymmetry $\mathbf{I}^{\odot}$ has already been measured at Jefferson Laboratory [67] for $\gamma\,\mathrm{p} \rightarrow \mathrm{p}\,\pi^+\,\pi^-$, and the analysis is continuing at present.

5.1 Measurement of Polarization Observables

The proposed experimental program will consist of four experiments with different combinations of beam and target polarization:

(A) **Linearly-polarized beam on a transversely-polarized target**
Measurement of $\mathbf{P}_{\mathbf{x}}^{\mathbf{s,c}}$, $\mathbf{P}_{\mathbf{y}}^{\mathbf{s,c}}$ (Equation 3 and Appendix B).

(B) **Circularly-polarized beam on a transversely-polarized target**
Measurement of $\mathbf{P}_{\mathbf{x}}^{\odot}$, $\mathbf{P}_{\mathbf{y}}^{\odot}$ (Equation 3 and Appendix B).

(C) **Linearly-polarized beam on a longitudinally-polarized target**
Measurement of $\mathbf{P}_{\mathbf{z}}^{\mathbf{s,c}}$ (Equation 3 and Appendix B).

(D) **Circularly-polarized beam on a longitudinally-polarized target**
Measurement of $\mathbf{P}_{\mathbf{z}}^{\odot}$ (Equation 3 and Appendix B).

5.1.1 Measurements with Circular Beam and Longitudinal Target Polarization

In the following, we will stick to the notation for polarization observables as proposed in Ref. [88]. For example, the 5-fold differential observable $\mathbf{P}_{\mathbf{z}}^{\odot}$ corresponds to the known observable $\mathbf{E}$ in single-meson production.

The reaction rate for $\gamma\,\mathrm{p} \rightarrow \mathrm{p}\,\pi^+\,\pi^-$, in the case of a circularly-polarized beam on a longitudinally-polarized target, can be written as:

$$\frac{\mathrm{d}\,\sigma}{\mathrm{d}\,x_i} = \sigma_0 \left\{ \left(1 + \Lambda_z \cdot \mathbf{P_z} \right) + \delta_{\odot} \left(\mathbf{I}^{\odot} + \Lambda_z \cdot \mathbf{P}_{\mathbf{z}}^{\odot} \right) \right\}. \tag{4}$$

In the following $\rightarrow$ and $\leftarrow$ indicate circular polarization of the beam in its two possible settings, $\Rightarrow$ and $\Leftarrow$ indicate long. target polarization parallel or anti-parallel to the beam:

$$(\rightarrow\Rightarrow - \leftarrow\Rightarrow) := \frac{\mathrm{d}\,\sigma(\rightarrow\Rightarrow)}{\mathrm{d}\,x_i} - \frac{\mathrm{d}\,\sigma(\leftarrow\Rightarrow)}{\mathrm{d}\,x_i} = 2 \cdot \sigma_0 \{\delta_\odot (\mathbf{I}^\odot + \Lambda_z \cdot \mathbf{P}_\mathbf{z}^\odot)\} \quad (5)$$

$$(\leftarrow\Leftarrow - \rightarrow\Leftarrow) := \frac{\mathrm{d}\,\sigma(\leftarrow\Leftarrow)}{\mathrm{d}\,x_i} - \frac{\mathrm{d}\,\sigma(\rightarrow\Leftarrow)}{\mathrm{d}\,x_i} = 2 \cdot \sigma_0 \{\delta_\odot (-\mathbf{I}^\odot + \Lambda_z \cdot \mathbf{P}_\mathbf{z}^\odot)\} \quad (6)$$

The latter two equations show that flipping only the beam is not sufficient to extract the double polarization observable $\mathbf{P}_\mathbf{z}^\odot$. The single polarization observable $\mathbf{I}^\odot$, only present in a three-particle final state, leads to an additional contribution. $\mathbf{I}^\odot$ does not depend on the target polarization and so occurs if only the beam is circularly polarized.

Equation 7 shows that flipping the beam and the target polarization is required to allow the measurement of $\mathbf{P}_\mathbf{z}^\odot$ by excluding the single polarization observable:

$$(\rightarrow\Rightarrow - \leftarrow\Rightarrow) + (\leftarrow\Leftarrow - \rightarrow\Leftarrow) := \frac{\mathrm{d}\,\sigma_{3/2}}{\mathrm{d}\,x_i} - \frac{\mathrm{d}\,\sigma_{1/2}}{\mathrm{d}\,x_i} = 4 \cdot \sigma_0 \cdot \delta_\odot \cdot (\Lambda_z \cdot \mathbf{P}_\mathbf{z}^\odot)\,. \quad (7)$$

Excluding the contribution from $\mathbf{I}^\odot$ is of special importance since background from the interaction of the polarized beam with the unpolarized target nucleons leads to an unknown asymmetry. This asymmetry could otherwise only be controlled by performing a background measurement using a circularly-polarized beam.

Information on $\mathbf{P_z}$ can be obtained from the same measurement:

$$(\leftarrow\Leftarrow - \leftarrow\Rightarrow) - (\rightarrow\Rightarrow - \rightarrow\Leftarrow) := -4 \cdot \sigma_0 \cdot (\Lambda_z \cdot \mathbf{P_z}) \quad (8)$$

For the measurement of $\mathbf{P}_\mathbf{z}^\odot$ and $\mathbf{P_z}$ it is of course necessary to determine the unpolarized differential cross section independently (preferably from a liquid hydrogen target), if one does not want to carry out extensive background measurements in order to be able to determine σ_0 from the double-polarization measurements.

The data from double-polarization experiments will provide extremely important information on baryons produced in photoproduction reactions, since individual partial waves are selectively suppressed or enhanced. It should be noted that all observables, such as invariant masses or angular distributions, will be affected by the polarization parameters. In addition, the asymmetries are significantly less sensitive to experimental uncertainties.

5.1.2 Measurements with Linear Beam and Longitudinal Target Polarization

For measurements with a linearly-polarized beam, the cross section can be written as

$$\frac{\mathrm{d}\,\sigma(\Rightarrow)}{\mathrm{d}\,x_i} = \sigma_0 \{(1 + \Lambda_z \cdot \mathbf{P_z}) + \delta_l [\sin 2\varphi (\mathbf{I^s} + \Lambda_z \cdot \mathbf{P_z^s}) + \cos 2\varphi (\mathbf{I^c} + \Lambda_z \cdot \mathbf{P_z^c})]\}\,. \quad (9)$$

Flipping the target spin yields

$$\frac{\mathrm{d}\,\sigma(\Leftarrow)}{\mathrm{d}\,x_i} = \sigma_0 \{(1 - \Lambda_z \cdot \mathbf{P_z}) + \delta_l [\sin 2\varphi (\mathbf{I^s} - \Lambda_z \cdot \mathbf{P_z^s}) + \cos 2\varphi (\mathbf{I^c} - \Lambda_z \cdot \mathbf{P_z^c})]\} \quad (10)$$

$$\frac{\mathrm{d}\,\sigma(\Rightarrow)}{\mathrm{d}\,x_i} - \frac{\mathrm{d}\,\sigma(\Leftarrow)}{\mathrm{d}\,x_i} = 2 \cdot \sigma_0 \cdot \Lambda_z \{(\mathbf{P_z}) + \delta_l [\sin 2\varphi (\mathbf{P_z^s}) + \cos 2\varphi (\mathbf{P_z^c})]\}\,. \quad (11)$$

In the difference the contribution from unpolarized nucleons drops out. What remains are only the contributions from polarized protons. Decomposing the measured cross section difference into terms following a $\cos 2\varphi$, $\sin 2\varphi$ dependence plus a constant, the observables ($\mathbf{P_z}$, $\mathbf{P_z^s}$, $\mathbf{P_z^c}$) can be extracted.

For the determination of $\mathbf{I^s}$ and $\mathbf{I^c}$ it is advantageous to use an LH_2 target rather than a butanol target to avoid problems due to the unpolarized nucleons in the butanol. Also in this case a decomposition into constant, $\cos 2\varphi$, and $\sin 2\varphi$ terms is necessary. Data with linearly-polarized photons on an unpolarized target were taken by the CLAS-g8b run group. These data are presently being analyzed and will provide an important understanding of the goniometer and thus, the production of linear polarization in double-polarization experiments.

5.1.3 Measurements with Transverse Target Polarization

For measurements with transverse target polarization, the polarization observables $\mathbf{P_{x,y}^{\odot}}$, $\mathbf{P_x^{s,c}}$, and $\mathbf{P_y^{s,c}}$ can be derived from Equation 2 in close analogy to the procedure described in sections 5.1.1 and 5.1.2.

5.2 Partial Wave Analysis

The main goal of a PWA is to identify the dynamical processes governing a reaction, to identify the intermediate baryon states, and to determine their quantum numbers and decay properties. This task is known to be difficult already in two-body final states, because technical problems may arise due to large interferences between amplitudes. Background contributions such as Born-terms, t, and also u-channel exchanges can play an important role, and must be taken into account (and projected onto each partial wave). The calculation of partial wave amplitudes for large data sets is generally time consuming and requires a lot of CPU power. The CLAS group at FSU maintains a 48-processor CPU grid node. It supports utilization of this grid HUB/PWA center presently dedicated for CLAS analyses.

Resonances have unique characteristics such as pole positions and decay couplings to different channels, which must be identical in all reactions. Fitting a set of reactions, like the π- and photo-induced production of one as well as two pions, allows the definition of a set of decay couplings which are directly connected to the width of the state. Therefore, it is important to do a combined analysis of different reactions and final states. The well known method of multiple decomposition is not suitable in this case since it cannot be directly applied to reactions with three or more particles in the final state.

For three-particle final states, the following techniques can be applied in both meson and baryon spectroscopy in order to perform a partial wave decomposition. The Zemach formalism and helicity formalism are well known examples where the calculation of angular dependences is performed via expansion into spherical harmonics, and their subsequent decomposition into Legendre polynomials. Both formalisms are often used in phenomenological analyses in a noncovariant form. In the helicity formalism, the spin rotation functions $D^J_{m\,m'}$ are used for the angular dependence. The helicity amplitude is intrinsically noncovariant because the spin $D^J_{m\,m'}$ functions are often expressed in the rest frame of each resonance. However, the decay probability of a certain configuration, given as the square of the amplitude, should be independent of any particular frame, i.e. a Lorentz scalar. Adjusting the helicity formalism requires the calculation of many rotations and Lorentz boosts. The use of covariant spin formalisms is needed to obtain reliable results [90].

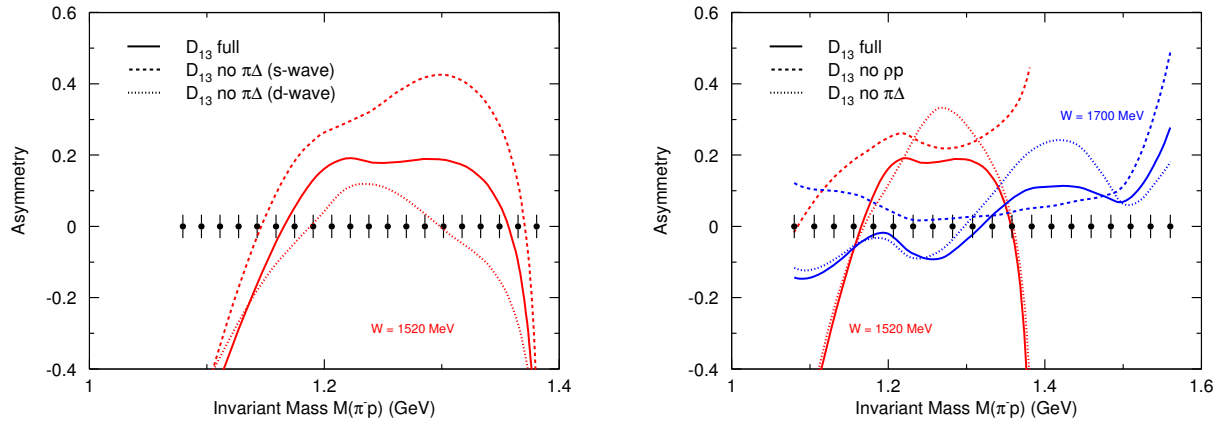

Figure 12: **Predictions for $P_z^{\odot}$ (called E in standard notation for single-meson production) based on a model by A. Fix for a circularly-pol. beam on a long.-pol. target.**

The covariant tensor formalism, which can be written in a relativistically invariant form based on kinematic factors related to the momenta of incoming and outgoing particles [63]. The fully covariant tensor formalism is often referred to as the Rarita-Schwinger formalism because usually one recalls a brief paper of these authors [91] in which the importance of the spin-tensor orthogonalization to the 4-velocity of the decaying system was stressed. This formalism can be applied if a particle with spin decays to one spinless meson and a resonance with spin. The energy dependence of the amplitude is parametrized in terms of analytic functions. This is especially important near the production threshold of a new state. The developed technique can be employed for the combined analysis of different channels, where the same coupling constants are used and amplitudes differ only by isospin coefficients. The method does not require additional Lorentz boosts, as opposed to the Zemach or helicity formalisms.

Formulae connecting the helicity and multipole decomposition were calculated [92, 93]. In case of a two-body final state, the covariant tensor formalism (also called operator formalism) can be rewritten in terms of a standard multipole decomposition [63]. A group at Carnegie-Mellon University has recently adopted the idea and has developed a PWA program also based on the covariant tensor formalism [94]. The structure of the C++ program allows easy access and thus facilitates extensions.

The CMU PWA code was designed to perform event-based maximum likelihood fits. In an event-based analysis, covariant amplitudes are calculated for all data, raw and accepted monte carlo events. The fit then finds the set of parameters which maximize the probability that the events measured were sampled, via detector acceptance, from a set of events governed by the physics of the input partial waves. These parameters, along with the covariant amplitudes, can be used to weight the raw monte carlo to obtain any acceptance corrected distribution or quantity (e.g. total cross section, dalitz plots, differential cross section vs. any kinematic variable, ...). A detailed description of the procedure and its successful application to CLAS data is given in the CLAS-Approved Analysis on *Baryon Spectroscopy Using CLAS Data from the g1c/g11 Data Sets*.

For the analysis of double-polarization data, we propose to perform an event-based maximum likelihood analysis of the unpolarized CLAS data (CMU analysis) obtained with a

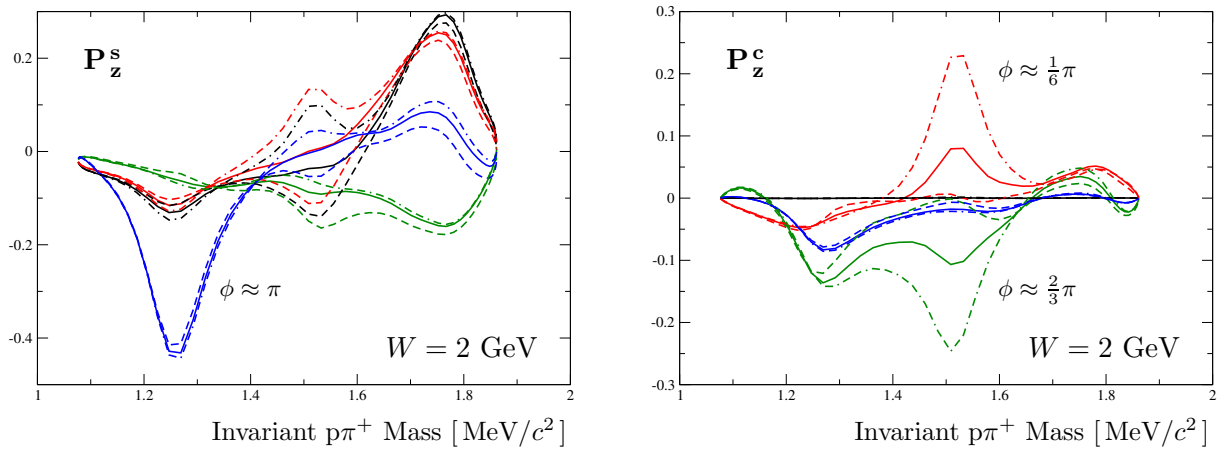

Figure 13: **Predictions of $\mathbf{P_z^s}$ (left) and $\mathbf{P_z^c}$ (right) by W. Roberts for a linearly-polarized beam on a longitudinally-polarized target.** *The different colors correspond to different values of ϕ (π^+ azimuthal angle in the rest frame of the $\pi^+\pi^-$ system.): $\phi \approx 0$ (black), $\phi \approx \frac{1}{6}\pi$ (red), $\phi \approx \frac{2}{3}\pi$ (green), and $\phi \approx \pi$ (blue). Furthermore, different line styles for each color represent different couplings (g_1 and g_2) of the $D_{13}(1520)$ to $\Delta\pi$ in S-wave and D-wave, respectively. The solid curves correspond to $g_1 = -0.47,\ g_2 = -3.34$, the dashed curves to $g_1 = -1.41,\ g_2 = 0.$, and the dot-dashed curves are for $g_1 = 0,\ g_2 = -10.104$.*

LH_2 target in combination with a χ^2-based fit of the large set of projections of the 5-fold polarization observables. Data taken using the butanol target has the added complication of an unpolarized nucleon background which would make an event-based analysis difficult. Fortunately, the CMU code can be easily upgraded to perform event-based and χ^2-based fits simultaneously. During each iteration of the event-based fit, the current set of parameters, along with the covariant amplitudes and a spin-density matrix, could be used to weight the raw Monte Carlo (MC). From the weighted MC each observable can be calculated and compared to the measured values to obtain a χ^2. The fit would then minimize the sum of the negative log likelihood and the weighted χ^2 values (the weights would depend on the relative weight of each observable in the fit).

6 Sensitivity Studies

We have studied the sensitivity of some double-polarization observables to certain resonances using two different models. In particular, the following sections describe the studies on the decay of the $D_{13}(1520)$ in the 1500 MeV/c^2 mass region as well as the study on resonances in the 1900 MeV/c^2 mass region.

Sensitivity to the $D_{13}(1520)$ S- and D-wave $\Delta\pi$ Decay

Fig. 12 shows predictions based on a model by Fix and Arenhovel [69]. In the left plot for $W = 1520$ MeV, the observable $\mathbf{P_z^\odot}$ is plotted versus the invariant $p\pi^-$ mass. The right plot shows the same illustration for an additional W of 1700 MeV (blue curves). The solid curve in each plot represents the full calculation, whereas the other curves describe the sensitivity of the observable to a variety of different contributions. The conclusion from these plots is that we can allow for an absolute error of 0.05 for the observable $\mathbf{P_z^\odot}$ in order to distinguish

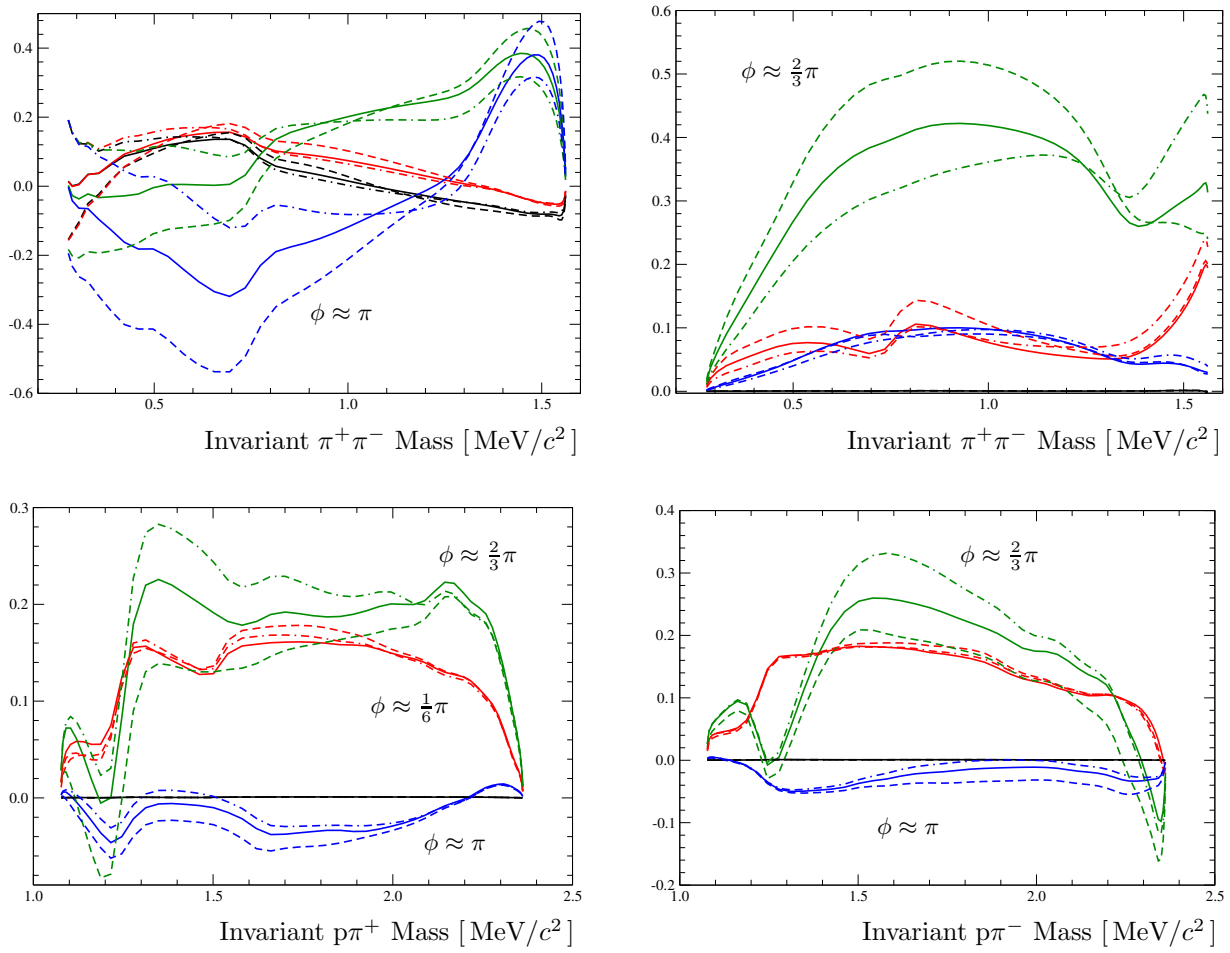

Figure 14: **Model calculations by W. Roberts for circularly-polarized beam and transverse target polarization for different kinematic variables [73]** *The top row shows predictions for the double-polarization observable* $\mathbf{P}_{\mathbf{x}}^{\odot}$ *(left) and* $\mathbf{P}_{\mathbf{y}}^{\odot}$ *(right) plotted versus the invariant mass of the two pions. The bottom row shows predictions for the observable* $\mathbf{P}_{\mathbf{y}}^{\odot}$ *plotted versus the invariant mass of the proton and the* π^+ *(left) as well as plotted versus the invariant mass of the proton and the* π^- *(right). The solid curves correspond to the full calculation, whereas the dashed curves arise when the* $S_{31}(1900)$ *is omitted from the calculation and the dot-dashed curves arise when the* $P_{31}(1910)$ *is omitted from the calculations. The black curves are at* $\phi \approx 0$*, the red curves are at* $\phi \approx \frac{1}{6}\pi$*, the green curves are at* $\phi \approx \frac{2}{3}\pi$*, and the blue curves are at* $\phi \approx \pi$*. The curves show strong effects in the variable* ϕ *which is defined as the* π^+ *azimuthal angle in the rest frame of the* $\pi^+\pi^-$ *system (helicity frame). See text for details.*

between a dominant S-wave or D-wave decay of the $D_{13}(1520)$ into $\Delta\pi$ (the error of 0.05 is indicated in Fig. 12 as a horizontal band assuming 20 invariant-mass bins).

Fig. 13 on the other hand shows the sensitivity of the observables $\mathbf{P}_{\mathbf{z}}^{\mathbf{s,c}}$ to the same process using a model by W. Roberts [73]. The observables are plotted versus the invariant pπ^+ mass. Here, the black curves are at $\phi \approx 0$, the red curves are at $\phi \approx \frac{1}{6}\pi$, the green curves are at $\phi \approx \frac{2}{3}\pi$, and the blue curves are at $\phi \approx \pi$, where ϕ is defined as the π^+ azimuthal angle in the rest frame of the $\pi^+\pi^-$ system (helicity frame). The different curves for each color correspond to different couplings of the $D_{13}(1520)$ to its decays into $\Delta\pi$ in S-wave and D-wave (see figure caption for details). We conclude that the observables depend strongly on

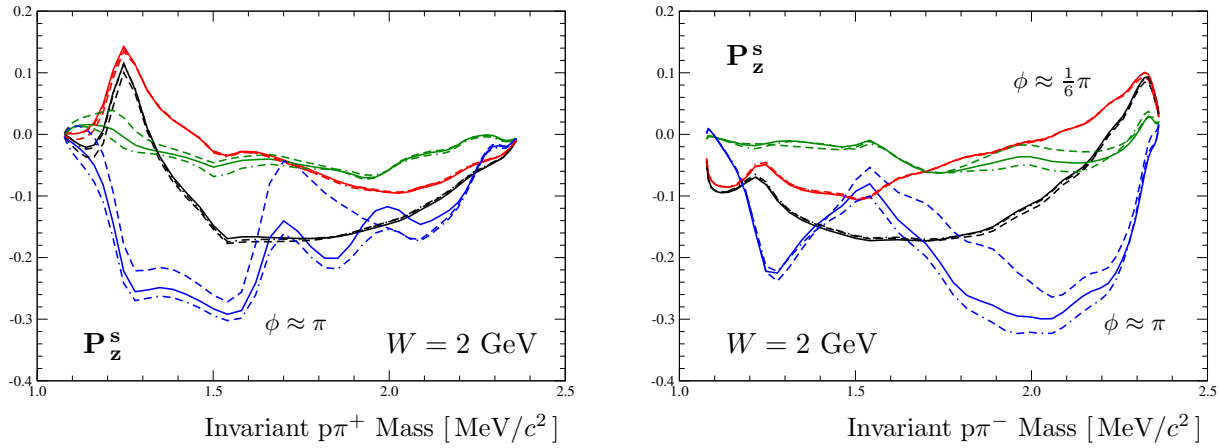

Figure 15: **Predictions of $\mathbf{P}_z^s$ by W. Roberts for a linearly-polarized beam on a longitudinally-polarized target.** *The color coding and line style is the same as in Fig. 14.*

the kinematical situation. An absolute error of 0.05 will be sufficient to study the decay of the $D_{13}(1520)$ over a wide mass range of the $p\pi^+$ system including different values of ϕ.

Sensitivity to $S_{31}(1900)$ or $P_{31}(1910)$

In the following, we studied the sensitivity of some polarization observables to contributions from resonances in the 1900 MeV/c^2 mass region. In particular, Fig. 14 shows model predictions for the double-polarization observables $\mathbf{P}_{x,y}^{\odot}$ and how these differ from the full solution if for example the $S_{31}(1900)$ (dashed curves) or the $P_{31}(1910)$ (dot-dashed curves) are omitted from the calculation. Fig. 15 shows predictions for the observable $\mathbf{P}_z^s$. In many plots that are functions of the invariant $p\pi^+$ or $p\pi^-$ mass, structures indicate the presence of the $\Delta(1232)$, but it has to be pointed out that much more than such a *visual* identification will be needed in the interpretation of any data obtained. In other plots that are functions of the $\pi^+\pi^-$ invariant mass, similar *structures* can be seen that identify the ρ meson. Note that in all these calculations no other $\pi^+\pi^-$ resonances are included, e.g. f_0 and σ contributions were omitted at this time. The plots are largely independent of the photocouplings of the excited baryons, indicating that contributions in which the excited baryon couples to the proton are small. We expect great sensitivity to the couplings of the resonances to the $\Delta\pi$ channel, particularly things like S/D (or P/F) ratios [95]. No baryons with spin greater than 3/2 have been included, but all resonances below 1.94 GeV/c^2 were considered.

We note that the observables are very sensitive to particular kinematic variables and in some cases, exhibit large values. The conclusion from these investigations is that we should allow for an absolute error of 0.05 in order to study the 1900 MeV/c^2 mass region. For some values of the angle ϕ, even an error of 0.1 will be sufficient (Fig. 14, top right: $\phi \approx \frac{2}{3}\pi$). However, all beam time requests given in Table 5 are based on a conservative error estimate of 0.05.

7 Acceptance Studies and Run Conditions

Identification of $\gamma\,p \rightarrow p\,\pi^+\,\pi^-$and Reconstruction Efficiency

We have considered two main sources of background. Single η or ω photoproduction may contribute with a neutral pion or a corresponding decay photon escaping detection. However,

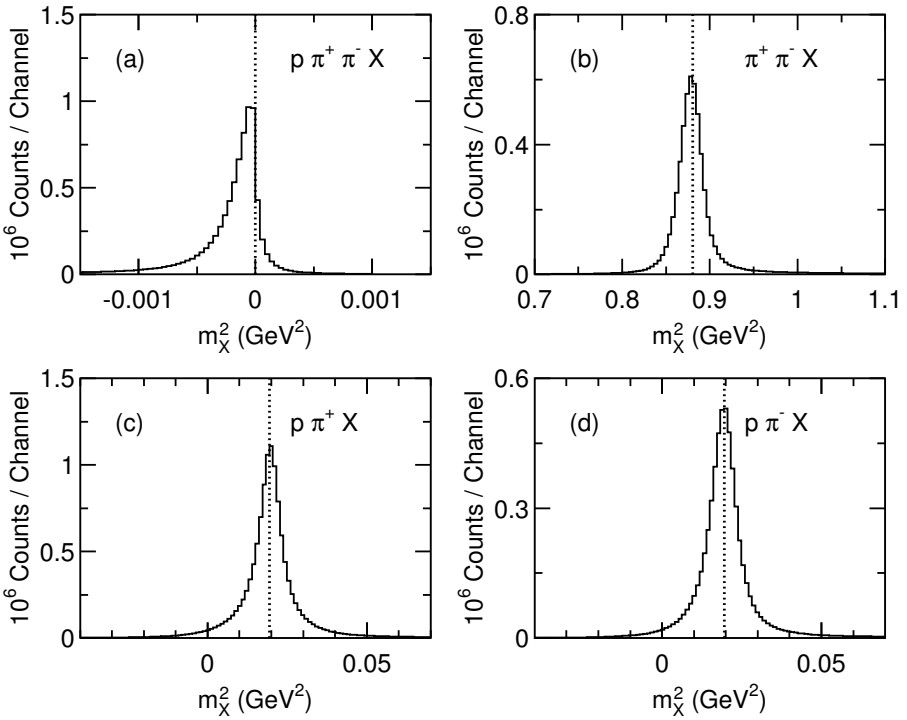

Figure 16: **Missing mass distributions when at least two charged particles are detected** *CLAS data were taken using a circularly-polarized tagged photon beam and an unpolarized target (g1c data set). At least two out of three particles in the final state are detected and the missing mass calculated. The distributions are essentially background free and thus, all expected background will come from the butanol target itself.*

Fig. 16 shows that the missing mass distributions on an unpolarized target (g1c data set) are basically background free.

In butanol, there are some additional reactions on the neutron, which are not present in the free-proton case, e.g. $\gamma n \to p\pi^-\pi^0$. This reaction matches one of our topologies when the proton and a π^- are detected. However, neutrons are all unpolarized and thus, these contributions to the asymmetries drop out (Eqs. 7, 8, and 11). This kind of background is taken care of by the effective dilution factor.

In our simulations, the final-state particles p, π^+, and π^- were generated according to a three-body phase-space distribution for photon energies between 400 MeV and 2000 MeV. A particle has been considered as detected if its direction fell within the (charge dependent) fiducial region of CLAS (assuming a torus current of 1920 A, compatible to the other FROST experiments) and the particle momenta exceeded 350 MeV/c for protons or 140 MeV/c for pions. The reaction was considered to be identified if two out of the three final-state particles were detected.

Figure 17 shows examples of the estimated CLAS acceptance. Panel (a) shows the average acceptance as a function of W. The acceptance is exceeding 0.50 for higher photon energies; it is smaller below about $W = 1.5$ GeV. An average acceptance of 0.5 has been assumed for the count-rate estimates. Panels (b) and (c) show the acceptance as a function of the invariant mass of the $p\pi^+$ system and as a function of the cosine of the proton polar angle in the center-of-mass system for a particular value of $W = 1.520$ GeV. Panel (c) demonstrates

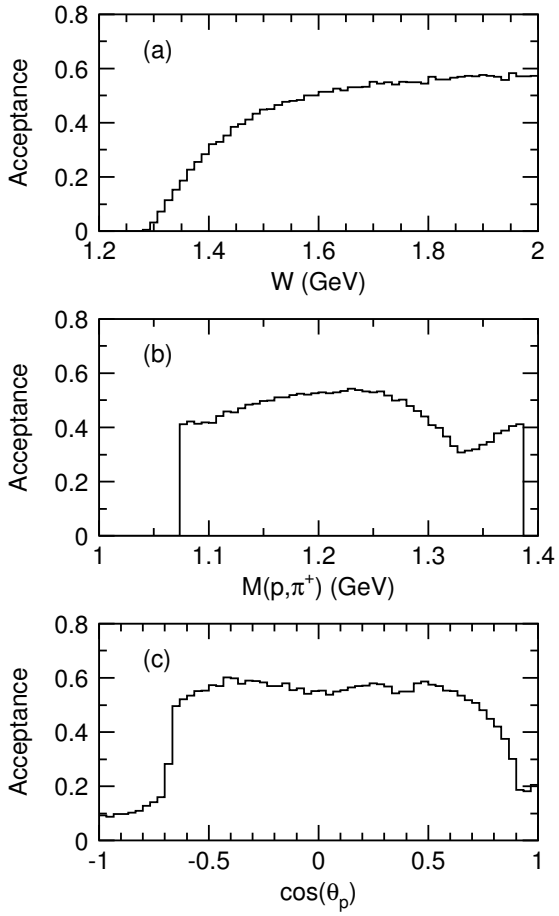

Figure 17: *Average acceptance of the CLAS spectrometer for the* $\gamma\, p \rightarrow p\,\pi^+\,\pi^-$ *reaction as a function of* W *when detecting at least two out of the three final state particles (a). Panels (b) and (c) illustrate the acceptance for a particular value of* $W = 1.520$ *GeV. The acceptance is plotted as a function of the invariant mass of the* $p\pi^+$ *system and as a function of the cosine of the proton polar angle in the center-of-mass system.*

that we will cover in the proposed measurements the full angular range in $\cos(\theta_{\rm p})$ with appreciable acceptances, on average larger than 0.20.

For measurements with a polarized target, additional background has to be considered: an enhanced background from electromagnetic processes and a contamination caused by $\pi^+\pi^-$ production on bound nucleons in the butanol (C_4H_9OH). The electromagnetic background needs to be suppressed on the trigger level. The contribution from unpolarized nucleons will dominate the background distribution in the $\gamma\,{\rm p} \rightarrow {\rm p}\,\pi^+\,\pi^-$ channel.

Background from Unpolarized Nucleons

For the measurements with a polarized target, butanol is used, which has an effective density of 0.61 g/cm^3 (see properties of butanol in Tab. 3). The polarization for protons in a butanol target will be about $P_z = 90\,\%$, but the fraction of protons that can be polarized (^{1}H atoms) is given by the naive dilution factor of $D = 10/74 \approx 14\,\%$. Hence, background from unpolarized nucleons in the carbon or oxygen nuclei of butanol is to be expected. Since the effective dilution factor $D_{\rm eff}^{-1} = 1 + r_{s/b}^{-1}$ ($r_{s/b}$: signal to background ratio) differs from the naive dilution factor of $D = 10/74$ and depends on the kinematics, it is impossible to subtract the background from the unpolarized nucleons easily. Therefore, it is necessary to flip the spin of the target and/or the beam and to measure the difference of cross sections as described in section 5. In this case, the contribution of unpolarized nucleons to the asmmetries drops out. It is of course also necessary to measure the unpolarized cross sections for normalization

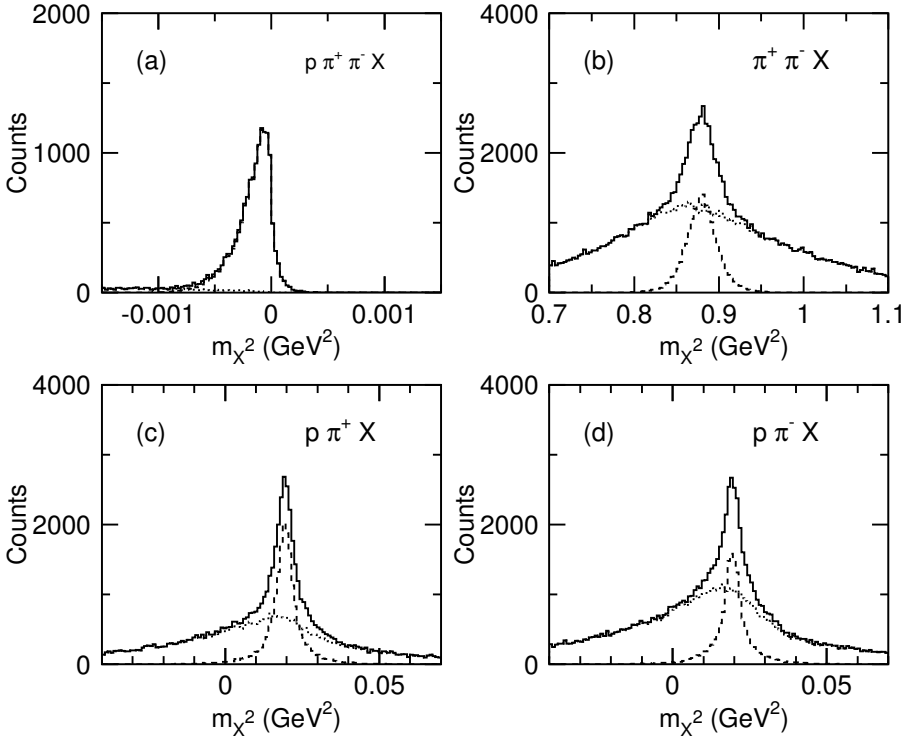

Figure 18: **Determination of the effective dilution factor in Monte Carlo simulations** *The plots show the missing mass distributions for the four event topologies. The total number of events is given by the solid line, whereas the dashed and dotted lines show the contributions from polarized hydrogen and unpolarized nucleons, respectively. See text for details.*

purposes in order to finally extract the polarization observables. These cross sections will be determined using the unpolarized g1c/g11 CLAS data.

The Fermi motion of the unpolarized nucleons in the quasi-free kinematics contributes to a broad background underneath the missing-mass distributions for events on hydrogen. However, on applying the same reconstruction procedure as for a pure hydrogen target, the tails of this Fermi energy smearing are cut off such that the background is strongly reduced. In Fig. 18, some results on our dilution factor studies are presented. The plots show the missing mass distributions for the four event topologies, i.e. either all three final-state particles are detected or any two out of three. A flat photon-energy distribution between 400 MeV and 2000 MeV was chosen and three-body phase-space distribution for the $p\pi^+\pi^-$ final state. The Fermi motion has been simulated in a standard way using a Gaussian distribution with $\sigma = 80$ MeV for the three momentum components of the initial unpolarized target nucleon as well as Gaussian distributions for the three momentum components of all detected particles with a σ of 5 MeV/c. Fig. 18 a (all three particles are detected) yields a dilution factor of 0.05 applying a cut of [-0.0010, 0.0005] GeV^2 on the asymmetric signal. Events were not included if the target was sampled to be an unpolarized neutron as no direct reaction on the neutron can result in the $p\pi^+\pi^-$ final state. One could think of charge-exchange reactions with other nucleons in the nucleus. These effects would, however, shift the background even further. Fig. 18 b (π^+ and π^- are detected) yields a dilution factor of 0.27 with a cut on the signal of [0.80, 0.95] GeV^2. Background events from both, protons and neutrons, contribute. We assumed that the cross sections for $\gamma p \to p\pi^+\pi^-$ and $\gamma n \to n\pi^+\pi^-$ are equal. The

dilution factor shows a factor of 2 improvement relative to the naive value of $D = 10/74$. This improvement was seen in the other FROST proposals, too. In Fig. 18 c (p and π^+ are detected), the dilution factor is 0.44 applying a cut on the signal of [0.00, 0.04] GeV^2. The dilution factor is increased as reactions on the neutron can not directly contribute to the $p\pi^+$ (X = π) final state. Finally, Fig. 18 d (p and π^- are detected) yields a dilution factor of 0.29 with a cut on the signal of [0.00, 0.04] GeV^2, again assuming that the cross sections for $\gamma p \to p\pi^+\pi^-$ $\gamma n \to n\pi^+\pi^-$ are equal. If we combine the total number of events within the cut regions in all four topologies, we obtain an effective dilution factor of 0.38. This includes the different acceptances for the various event topologies. With a smaller Fermi momentum of 70 MeV, we get a slightly worse combined dilution factor of 0.35. In the approved proposal E03-105 [3], the dilution factor was estimated to be $D \approx 0.43$ for single-pion photoproduction based on γp reactions (g1c data) relative to $\gamma\,^4$He reactions (g3a data).

There is a chance that we can reduce further nuclear background in the analysis of real experimental data by applying additional event-selection criteria and kinematical cuts. Rejection of events with more than one proton detected in CLAS may be an option, for instance. The asymmetries of reactions on free protons can be different from those on bound nucleons. In the analysis of the real data, we will evaluate and subtract background in each kinematical bin. To get a better handle on the background from bound nuleons, we are planning to install an additional carbon target with a thickness of about $10 - 20$ % of the main target, located a few centimeters downstream of the polarized target. Thus, we will be able to measure simultaneously events from both targets. In the analysis, we can then clearly separate events by using vertex information.

Trigger

We will run with the torus magnetic field set to one-half of the maximum field, outbending positive particles. For the proposed experiment, the *ideal* trigger would require the detection of at least two charged particles. This is in agreement with the experiment E02-112 [2] which has 20 days approved for measurements with linearly polarized beam and transversely polarized target. For the other polarization configurations, we propose to use a trigger requiring at least one charged particle in CLAS. This trigger configuration is compatible with all other approved experiments using the frozen-spin target.

Estimate of Systematic Uncertainties

There are several main sources of systematic uncertainties. Among other things, these are beam polarization uncertainty, target polarization uncertainty, effective dilution factor uncertainty, instrumental asymmetry in the detector. To minimize effects of the instrumental asymmetry, we will flip beam and target polarization. The latter will also help to discriminate between polarized and unpolarized target nuclei. In case of circularly-polarized beam, the helicity flips continuously following helicity changes of the electron beam. The beam polarization can be determined to better than 4 % using a Møller Polarimeter to measure the polarization of the primary electron beam and the calculated helicity transfer. In case of linearly-polarized beam, we will rotate the polarization plane periodically by changing the orientation of the radiator crystal. In this case, the beam polarization can be determined via an analysis of the photon spectrum and a photon polarimeter. Target polarization will be flipped every time we do repolarization. A precise measurement of the target polarization

will be done in a high field when the target is inside of the polarizing magnet at the beginning and at the end of each repolarization cycle. We also will do polarization measurements periodically during an experimental run when the target is in holding field. To get better control of the effective dilution factor, we will install an additional carbon target and will take data from both targets simultaneously. We use the same estimates for uncertainties as described in other approved experiments (E02-112 [2] and E05-012 [5]). The estimates are as follows:

- Beam polarization 4 – 6 %
- Target polarization 3 – 4 %
- Dilution factor 5 %
- Photon flux on target 5 – 6 %
- Target Thickness 3 – 5 %

8 Count Rate Estimates and Statistical Uncertainties

8.1 Count Rate Estimate

The rate of reconstructed $\gamma\,\mathrm{p} \rightarrow \mathrm{p}\,\pi^+\,\pi^-$ events originating from free protons in the frozen-spin butanol target can be calculated using

$$N^{\mathrm{free}}_{\mathrm{p}\,\pi^+\,\pi^-} = \dot{N}_\gamma \cdot \rho^{\mathrm{p}}_{\mathrm{target}} \cdot \sigma^{\mathrm{p}}_{\mathrm{tot}} \cdot \epsilon \cdot \Gamma \cdot 1/N_{\mathrm{bins}} \tag{12}$$

where $\dot{N}_\gamma$ is the tagged photon rate, $\rho^{\mathrm{p}}_{\mathrm{target}}$ the target area density of free protons, $\sigma^{\mathrm{p}}_{\mathrm{tot}}$ the total cross section for the reaction on free protons, ϵ the reconstruction efficiency, Γ the branching fraction into the final-state particles, and N_{bins} the desired number of bins.

Besides reactions on free protons, we will also reconstruct unwanted background events from bound nucleons in the butanol molecules, though with a lower reconstruction efficiency. This is described by the effective dilution factor D_{eff}. The ratio of reconstructed events from free nucleons to reconstructed events from bound nucleons is given by

$$N^{\mathrm{free}}_{\mathrm{p}\,\pi^+\,\pi^-} \,/\, N^{\mathrm{bound}}_{\mathrm{p}\,\pi^+\,\pi^-} = D_{\mathrm{eff}}/(1 - D_{\mathrm{eff}})\,. \tag{13}$$

For this reason, we can calculate the total reconstructed event rate using

$$N^{\mathrm{tot}}_{\mathrm{p}\,\pi^+\,\pi^-} = N^{\mathrm{free}}_{\mathrm{p}\,\pi^+\,\pi^-} + N^{\mathrm{bound}}_{\mathrm{p}\,\pi^+\,\pi^-} = D^{-1}_{\mathrm{eff}} \cdot \dot{N}_\gamma \cdot \rho^{\mathrm{p}}_{\mathrm{target}} \cdot \sigma^{\mathrm{p}}_{\mathrm{tot}} \cdot \epsilon \cdot \Gamma \cdot 1/N_{\mathrm{bins}}\,, \tag{14}$$

where we can assume an average reconstruction efficiency of $\epsilon \approx 0.5$, an effective dilution factor of $D_{\mathrm{eff}} \approx 0.35$ (both numbers based on the Monte Carlo studies described in section 7), and a target area density of $\rho^{\mathrm{p}}_{\mathrm{target}} = 2.48 \cdot 10^{23}/\mathrm{cm}^2 = 2.48 \cdot 10^{-7}/\mu\mathrm{b}$ [1], which also includes the packing factor of 0.62. $\Gamma = 1.0$ for all particles. On the average, we are expecting about 2100 double-charged pion events per day for a given kinematical bin ($N_{\mathrm{bins}} = 2000$) and a total of approximately 4.2 million $\pi^+\pi^-$ events per day.

[1] $\rho^{\mathrm{p}}_{\mathrm{target}} = \rho_{\mathrm{tg}} \cdot l_{\mathrm{tg}} \cdot N_{\mathrm{A}} \cdot 10\,/\,A_{\mathrm{butanol}}$ using $l = 50$ mm, $\rho_{\mathrm{tg}} = 0.611$ g/cm^3, and $A_{\mathrm{butanol}} = 74.12$ g/mol

8.2 Uncertainties of the Measurements and Necessary Beam Time

In general, a double polarization observable **P** is proportional to an asymmetry A that arises as the difference of measurements with the spins of the incoming photons either aligned with the spins of the free protons in the target material ($\rightarrow\Rightarrow$ or $\leftarrow\Leftarrow$ configuration) or opposite to the free proton spins ($\leftarrow\Rightarrow$ or $\rightarrow\Leftarrow$ configuration). If we label the number of counts obtained in these measurements with $N_{\parallel}$ and $N_{\perp}$, respectively, the asymmetry is given by

$$A = \frac{1}{D_{\text{eff}} \cdot \delta \cdot \Lambda} \frac{N_{\parallel} - N_{\perp}}{N_{\parallel} + N_{\perp}} \tag{15}$$

and the statistical error can be determined using

$$\Delta A\,(\,\text{stat.}) \approx \frac{1}{D_{\text{eff}} \cdot \delta \cdot \Lambda} \frac{1}{\sqrt{N_{\parallel} + N_{\perp}}}\,. \tag{16}$$

Solving for the total number of counts required to reach a certain precision $\Delta A\,(\,\text{stat.})$ we obtain

$$\Rightarrow N_{\parallel} + N_{\perp} \approx \left(\frac{1}{D_{\text{eff}} \cdot \delta \cdot \Lambda \cdot \Delta A\,(\,\text{stat.})}\right)^2\,, \tag{17}$$

and thus, the beam time needed to reach a certain statistical accuracy ΔA is given by

$$T = \frac{1}{\dot{N}_{\gamma}(E)} \cdot \frac{1}{(\Delta A)^2} \cdot \frac{1}{\sigma_{\text{unpol}}} \cdot \frac{1}{\rho^{\text{p}}_{\text{target}} \cdot \epsilon} \cdot \frac{D^{-1}_{\text{eff}}}{(\delta \cdot \Lambda)^2} \cdot N_{\text{bins}}\,. \tag{18}$$

8.3 Rate Estimates

The total luminosity is restricted by maximum rates of the tagger, the data acquisition system, and accidental background. To ensure that the experimental rates are kept within those limits, we have adjusted the proposed photon flux assuming the parameters of Table 4 and the total cross section per nucleon shown in Figure 19. The total per-nucleon photo cross section on lead is a good approximation for the per-nucleon cross sections of the butanol target materials carbon and oxygen. The mean tagging efficiency was estimated by calculating the transmitted fraction through the collimator using tabulated bremsstrahlung angular distribution calculations ([3] and references therein). We are planning to run with a collimated photon beam the parameters of which were assumed in the calculations. For the circularly-polarized beam, the diameter of the passive collimator will be 2.6 mm at a distance of 5.8 m. Settings A and C with linearly-polarized photons will run with a collimator of 1.0 mm in diameter at a distance of 22.9 m from the goniometer. In case of coherent

Maximum tagger rate	30 MHz
Maximum tagger rate per T-counter	4-5 MHz
Maximum CLAS DAQ rate	3.5 kHz
Mean tagging efficiency (at $E_{\text{e}} = 1.6$ GeV)	0.18
Mean tagging efficiency (at $E_{\text{e}} = 2.2$ GeV)	0.48
Coincidence time window	15 ns
CLAS acceptance for a hadronic event	0.70

Table 4: **Parameters for rate estimates**

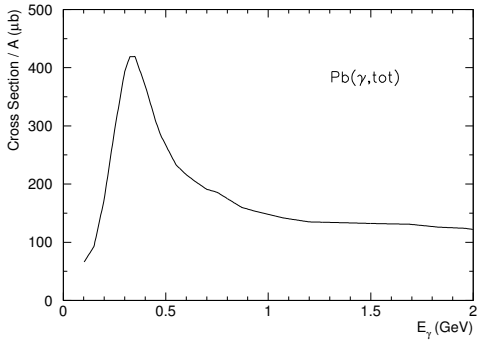

Figure 19: **Total γ + Pb cross section per nucleon taken from [3]**
The shown total per-nucleon photo cross section on lead is a good approximation for the per-nucleon cross sections of the butanol target materials carbon as well as oxygen.

bremsstrahlung, all the tagger rate is concentrated in a peak about 200-MeV wide that is covered just by a few T-counters. The polarization of the collimated beam is fairly constant over this 200 MeV energy range near the coherent edge. In fact, it diminishes by less than 5 % at 200 MeV below the coherent edge energy. For this reason, keeping all this in mind, we can run with $5 \cdot 10^6$ γ/s on target in the range of the coherent peak without overloading the tagger and DAQ, and still have an acceptable rate of accidental coincidences. For circularly-polarized photons the rates can be higher.

9 Summary and Beam Time Request

The experimental configuration is compatible with four other approved experiments on pion, eta and kaon photoproduction (E02-112, E03-105, E04-102, and E05-012). Proposed new beam/target settings are presented in Table 5. The beam time has been calculated using Eq. 18. Other already approved FROST experiments are summarized in Figure 20. It shows the total required time in addition to the time that has already been approved.

Linearly-Polarized Beam

Settings A and C: The required error has been estimated to 0.05 for both settings based on our sensitivity studies in section 6. For linear-beam polarization, most of the photon flux is confined to a 200-MeV wide interval. We have estimated a total number of $10 \cdot 20 \cdot 10 = 2000$ bins, i.e. 10 E_γ bins, 20 bins in $\mathrm{d}\sigma/\mathrm{d}x_i$ (for example any two-particle invariant mass), and 10 bins in ϕ. The required beam time has been calculated using Eq. 18. For setting A, higher energies ($E_\gamma > 2$ GeV) have been already well approved by previous PACs (see Fig. 20). For this reason, new beam time is not required. For setting C, more beam time at $E_\gamma = 2.0$ MeV, 2.2 MeV, 2.4 MeV, and 2.6 MeV is necessary (see Tab. 5) in order to cover a mass range up to 2.4 GeV/c^2, which will then allow for a proper study of (even broad) resonances at and above the 2 GeV/c^2 mass region (Fig. 13 and 15).

Circularly-Polarized Beam

Settings B and D: For a circularly-polarized beam, we have also estimated a required error of 0.05 (according to section 6) and a total number of 2000 bins. Thus, using Equation 18, the required new beam time for higher energies ($E_{e^-} = 3.1$ GeV corresponding to center-of-mass energies up to $W \approx 2.6$ GeV) is 100 hours for settings B and D, respectively (Tab. 5).

Setting	E [GeV]	$\sigma_{\text{tot}}^{\text{p}}$ [μb]	$\dot{N}_\gamma$ [MHz]	N_{bins}	$\delta_\odot/\delta_l$	Λ_{tg}	ΔA	T [h]
A								
B circ/trans	$E_{\text{e}^-} = 3.1$	≈ 35	≈ 3	2000	0.82	0.85	0.05	100
C lin/long	$E_{\gamma,\,\text{coh.}} = 2.0$	≈ 40	≈ 5	2000	0.7	0.85	0.05	72
	$E_{\gamma,\,\text{coh.}} = 2.2$	≈ 35	≈ 5	2000	0.7	0.85	0.05	83
	$E_{\gamma,\,\text{coh.}} = 2.4$	≈ 35	≈ 5	2000	0.7	0.85	0.05	83
	$E_{\gamma,\,\text{coh.}} = 2.6$	≈ 35	≈ 5	2000	0.7	0.85	0.05	83
D circ/long	$E_{\text{e}^-} = 3.1$	≈ 35	≈ 3	2000	0.82	0.85	0.05	100
								Σ 22 days

Table 5: **Required new beam time to study the reaction $\gamma\,\mathbf{p} \to \mathbf{p}\,\pi^+\,\pi^-$ above 2 GeV/c^2.** *However, we are aware of the already approved 84 days for FROST and feel committed to prove the success of the project before requesting these 22 days. See text below for more details.*

Beam Time Request

We are aware of the already approved 84 days for FROST and feel committed to prove the success of the project before requesting the full amount of beam time required for double-pion production at higher energies.

For this reason, we request only 4 days of beam time for setting B in this proposal. More time would be needed to carry out the complete double-pion experiment up to higher energies (Tab. 5). On the other hand, the additional constraints imposed by the obervables $\mathbf{P}_{\mathbf{x}}^{\odot}$ and $\mathbf{P}_{\mathbf{y}}^{\odot}$ will already greatly help improve our understanding of the important mass region at and above 2 GeV/c^2.

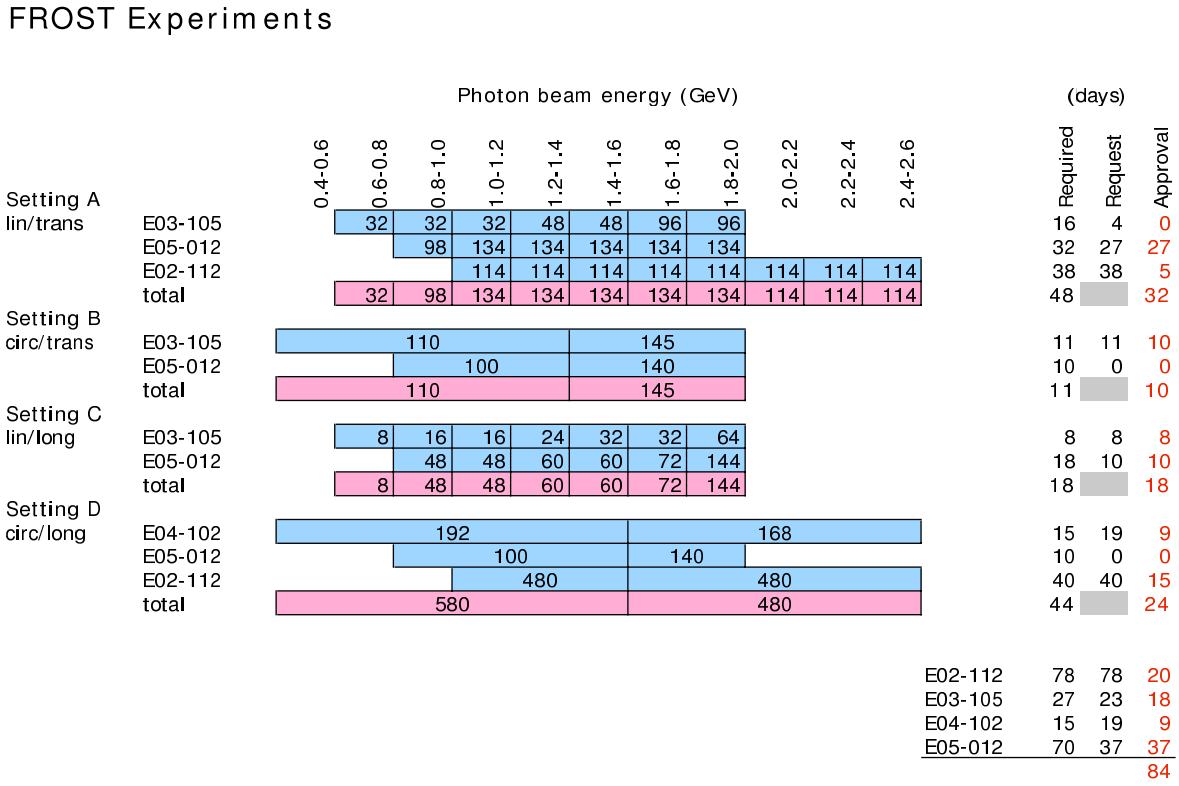

Figure 20: **Already approved FROST beam time**

A Theoretical Predictions

model state	$N\pi$	$N\eta$	$\sqrt{\Gamma^{tot}_{N\rho}}$	$\sqrt{\Gamma^{tot}_{\Delta\pi}}$	$A^p_{1/2}$	$A^p_{3/2}$
$[N\frac{1}{2}^-]_3(1945)$	$5.7^{+0.5}_{-1.6}$	$2.4^{+1.5}_{-2.3}$	$18.1^{+3.9}_{-7.3}$	$6.7^{+1.5}_{-1.3}$	12	–
$N\frac{1}{2}^-(2090)S_{11}$*	7.9 ± 3.8	–	14.2 ± 4.3	5.1 ± 5.9		
$[N\frac{1}{2}^-]_4(2030)$	$3.7^{+0.5}_{-1.1}$	$-1.0^{+1.5}_{-1.1}$	1.1 ± 0.4	$5.7^{+1.3}_{-1.1}$	20	–
$[N\frac{1}{2}^-]_5(2070)$	$2.1^{+0.8}_{-1.5}$	$0.1^{+0.3}_{-0.5}$	$7.8^{+1.7}_{-3.5}$	$13.1^{+3.3}_{-2.7}$	nc	–
$[N\frac{1}{2}^-]_6(2145)$	0.4 ± 0.1	$-0.4^{+0.4}_{-0.3}$	$2.3^{+1.4}_{-0.6}$	1.0 ± 0.2	nc	–
$[N\frac{1}{2}^-]_7(2195)$	0.1 ± 0.1	$-0.9^{+0.5}_{-0.3}$	$3.5^{+2.0}_{-0.5}$	2.1 ± 0.1	nc	–
$[N\frac{3}{2}^-]_3(1960)$	$8.2^{+0.7}_{-1.7}$	4.0 ± 0.2	$13.6^{+2.7}_{-5.8}$	$5.5^{+1.2}_{-1.0}$	nc	nc
$N\frac{3}{2}^-(2080)D_{13}$**	5.0 ± 2.5	–	10.7 ± 3.5	10.5 ± 4.2		
$[N\frac{3}{2}^-]_4(2055)$	$6.2^{+0.1}_{-0.6}$	$0.4^{+0.0}_{-0.1}$	$7.7^{+1.1}_{-3.9}$	$11.1^{+2.6}_{-2.2}$	16	0
$[N\frac{3}{2}^-]_5(2095)$	$0.2^{+0.1}_{-0.2}$	$-0.2^{+0.1}_{-0.0}$	$3.6^{+0.8}_{-1.4}$	$6.9^{+4.7}_{-1.1}$	−9	−14
$[N\frac{3}{2}^-]_6(2165)$	$1.5^{+0.1}_{-0.2}$	-2.4 ± 0.1	$1.7^{+0.9}_{-0.3}$	$3.1^{+0.9}_{-0.7}$	nc	nc
$[N\frac{3}{2}^-]_7(2180)$	$1.7^{+0.1}_{-0.2}$	-1.7 ± 0.1	$1.6^{+0.9}_{-0.2}$	$5.0^{+1.3}_{-1.1}$	nc	nc
$[N\frac{5}{2}^-]_2(2080)$	$5.1^{+0.2}_{-0.8}$	3.5 ± 0.4	$8.8^{+9.3}_{-3.0}$	$4.7^{+1.8}_{-0.8}$	−3	−14
$[N\frac{5}{2}^-]_3(2095)$	$5.2^{+0.4}_{-1.0}$	$0.0^{+0.4}_{-0.2}$	$2.3^{+2.4}_{-1.3}$	$7.9^{+1.2}_{-1.3}$	−2	−6
$N\frac{5}{2}^-(2200)D_{15}$**	4.5 ± 2.3	–	–	–		
$[N\frac{5}{2}^-]_4(2180)$	$1.9^{+0.1}_{-0.3}$	-1.1 ± 0.0	$2.2^{+1.2}_{-0.3}$	$6.2^{+2.1}_{-1.5}$	nc	nc
$[N\frac{5}{2}^-]_5(2235)$	$2.0^{+0.1}_{-0.3}$	$0.6^{+0.0}_{-0.1}$	$4.0^{+2.4}_{-1.0}$	$7.0^{+5.1}_{-3.2}$	nc	nc
$[N\frac{5}{2}^-]_6(2260)$	0.4 ± 0.1	$0.1^{+0.1}_{-0.0}$	$2.9^{+1.1}_{-0.8}$	$7.1^{+1.5}_{-1.6}$	nc	nc
$[N\frac{5}{2}^-]_7(2295)$	0.2 ± 0.1	$-1.6^{+0.3}_{-0.1}$	$2.8^{+1.7}_{-1.4}$	$4.9^{+1.0}_{-1.2}$	nc	nc
$[N\frac{5}{2}^-]_8(2305)$	0.3 ± 0.1	$-0.6^{+0.1}_{-0.0}$	$1.8^{+0.6}_{-0.7}$	$5.2^{+1.5}_{-1.4}$	nc	nc
$[N\frac{7}{2}^-]_1(2090)$	6.9 ± 1.3	2.5 ± 0.7	$12.1^{+4.8}_{-1.4}$	$2.9^{+1.3}_{-0.9}$	−34	28
$N\frac{7}{2}^-(2190)G_{17}$****	7.0 ± 3.0	–	12.5 ± 1.2	–		
$[N\frac{7}{2}^-]_2(2205)$	4.0 ± 1.1	-0.1 ± 0.0	$3.2^{+3.3}_{-1.1}$	$6.5^{+4.1}_{-2.5}$	−16	4
$[N\frac{7}{2}^-]_3(2255)$	0.8 ± 0.2	0.0	$2.4^{+2.1}_{-1.1}$	$11.9^{+1.6}_{-2.3}$	nc	nc
$[N\frac{7}{2}^-]_4(2305)$	0.4 ± 0.1	-0.8 ± 0.3	$2.0^{+0.3}_{-0.7}$	$4.3^{+2.8}_{-2.0}$	nc	nc
$[N\frac{7}{2}^-]_5(2355)$	1.1 ± 0.3	$+0.4 \pm 0.1$	$2.4^{+0.6}_{-0.7}$	0.9 ± 0.1	nc	nc
$[N\frac{9}{2}^-]_1(2215)$	2.5 ± 0.3	-2.1 ± 0.4	$1.8^{1.0}_{-0.7}$	$6.3^{+2.3}_{-1.8}$	0	1
$N\frac{9}{2}^-(2250)G_{19}$****	5.9 ± 1.9	–	–	–		

Table 6: **Results for the lightest few negative-parity nucleon resonances**
Results are for the lightest negative-parity resonances of each J in the N=3 band in the $N\pi$, $N\eta$, $N\rho$, *and* $\Delta\pi$ *channels. Notation for model states is* $[J^P]_n$ *(mass [MeV]), with* J^P *the spin/parity of the state and n its principal quantum number. The first rows give the model results of Capstick and Roberts [75], while the second row lists the corresponding numbers obtained by Manley and Saleski in their partial wave analysis [78], the PDG name,* $N\pi$ *partial wave, and the star rating. The square of the listed amplitude value yields the partial width in [MeV]. The last two columns list the helicity couplings of the proton given in* 10^{-3} $GeV^{-1/2}$, *nc = not calculated [27].*

$J\pi$	$M^{'}$	Resonance$^{\rm exp}$	$\Gamma^{\rm exp}$	$\Gamma^{\rm theory}$
$1/2+$	1539	N(1440^{+30}_{-10}), 4^*	88^{+48}_{-38}	33
$1/2+$	1741	N(1710^{+30}_{-30}), 3^*	28^{+73}_{-20}	44
$3/2+$	1938	N(1900^{+0}_{-38}), 2^*		4.4
$3/2+$	1990	missing		22
$3/2+$	2012	missing		7.1
$5/2+$	1721	N(1680^{+10}_{-5}), 4^*	13^{+8}_{-7}	3.5
$5/2+$	1989	missing		7.7
$5/2+$	2005	missing		18
$7/2+$	1994	missing		9.0
$1/2-$	1678	N(1650^{+30}_{-10}), 4^*	6^{+7}_{-5}	5.3
$1/2-$	1940	missing		11
$3/2-$	1477	N(1520^{+10}_{-5}), 4^*	24^{+10}_{-8}	35
$3/2-$	1633	N(1700^{+50}_{-50}), 3^*	seen	88
$3/2-$	1929	missing		9.7
$3/2-$	2175	missing		3.2
$5/2-$	1657	N(1675^{+10}_{-5}), 4^*	83^{+26}_{-13}	30
$5/2-$	2180	missing		2.1
$5/2-$	2195	missing		5.7
$7/2-$	2195	N(2190^{+10}_{-90}), 4^*		11
$9/2-$	2193	N(2250^{+60}_{-80}), 4^*		8.6
$3/2+$	1872	missing		3.6
$5/2+$	1898	$\Delta(1905^{+15}_{-35})$, 4^*	44^{+66}_{-44}	15
$5/2+$	1984	$\Delta(2000^{+325}_{-280})$, 2^*	seen	13
$5/2+$	2307	missing		2.2
$7/2+$	1956	$\Delta(1950^{+10}_{-10})$, 4^*	75^{+30}_{-17}	17
$7/2+$	2339	$\Delta(2390^{+95}_{-140})$, 1^*		3.4
$1/2-$	1654	$\Delta(1620^{+55}_{-5})$, 4^*	68^{+41}_{-32}	72
$1/2-$	2099	$?\Delta(1900^{+50}_{-50})$, 2^*	seen	7.0
$3/2-$	1628	$\Delta(1700^{+70}_{-30})$, 4^*	135^{+105}_{-75}	52
$3/2-$	2089	$?\Delta(1940^{+227}_{-100})$, 1^*	seen	3.6
$5/2-$	2209	missing		7.6
$7/2-$	2180	missing		3.4
$7/2-$	2238	$\Delta(2200^{+160}_{-80})$, 1^*		3.7

Table 7: **$\Delta\pi$ decay widths [1] for several N* in a relativistic quark model based on instantons [12].** *Only states with a $\Delta\pi$ width larger than 3 MeV are shown. The helicity couplings are also calculated within this model but not available, yet.*

B Polarization Observables for Double–Pion Photoproduction

Observable	Helicity Form	Experiment
I_0	$\lvert\mathcal{M}_1^-\rvert^2 + \lvert\mathcal{M}_1^+\rvert^2 + \lvert\mathcal{M}_2^-\rvert^2 + \lvert\mathcal{M}_2^+\rvert^2$ $+\lvert\mathcal{M}_3^-\rvert^2 + \lvert\mathcal{M}_3^+\rvert^2 + \lvert\mathcal{M}_4^-\rvert^2 + \lvert\mathcal{M}_4^+\rvert^2$	unpolarized photon beam
$I_0\,P_x$	$2\,\Re\,(\mathcal{M}_1^-\,\mathcal{M}_3^{-\,*} + \mathcal{M}_1^+\,\mathcal{M}_3^{+\,*} + \mathcal{M}_2^-\,\mathcal{M}_4^{-\,*} + \mathcal{M}_2^+\,\mathcal{M}_4^{+\,*})$	
$I_0\,P_y$	$-2\,\Im\,(\mathcal{M}_1^-\,\mathcal{M}_3^{-\,*} + \mathcal{M}_1^+\,\mathcal{M}_3^{+\,*} + \mathcal{M}_2^-\,\mathcal{M}_4^{-\,*} + \mathcal{M}_2^+\,\mathcal{M}_4^{+\,*})$	
$I_0\,P_z$	$-\lvert\mathcal{M}_1^-\rvert^2 - \lvert\mathcal{M}_1^+\rvert^2 - \lvert\mathcal{M}_2^-\rvert^2 - \lvert\mathcal{M}_2^+\rvert^2$ $+\lvert\mathcal{M}_3^-\rvert^2 + \lvert\mathcal{M}_3^+\rvert^2 + \lvert\mathcal{M}_4^-\rvert^2 + \lvert\mathcal{M}_4^+\rvert^2$	
$I_0\,I^{\odot}$	$-\lvert\mathcal{M}_1^-\rvert^2 + \lvert\mathcal{M}_1^+\rvert^2 - \lvert\mathcal{M}_2^-\rvert^2 + \lvert\mathcal{M}_2^+\rvert^2$ $-\lvert\mathcal{M}_3^-\rvert^2 + \lvert\mathcal{M}_3^+\rvert^2 - \lvert\mathcal{M}_4^-\rvert^2 + \lvert\mathcal{M}_4^+\rvert^2$	circularly polarized photons
$I_0\,P_x^{\odot}$	$2\,\Re\,(-\mathcal{M}_1^-\,\mathcal{M}_3^{-\,*} + \mathcal{M}_1^+\,\mathcal{M}_3^{+\,*} - \mathcal{M}_2^-\,\mathcal{M}_4^{-\,*} + \mathcal{M}_2^+\,\mathcal{M}_4^{+\,*})$	
$I_0\,P_y^{\odot}$	$2\,\Im\,(\mathcal{M}_1^-\,\mathcal{M}_3^{-\,*} - \mathcal{M}_1^+\,\mathcal{M}_3^{+\,*} + \mathcal{M}_2^-\,\mathcal{M}_4^{-\,*} - \mathcal{M}_2^+\,\mathcal{M}_4^{+\,*})$	
$I_0\,P_z^{\odot}$	$\lvert\mathcal{M}_1^-\rvert^2 - \lvert\mathcal{M}_1^+\rvert^2 + \lvert\mathcal{M}_2^-\rvert^2 - \lvert\mathcal{M}_2^+\rvert^2$ $-\lvert\mathcal{M}_3^-\rvert^2 + \lvert\mathcal{M}_3^+\rvert^2 - \lvert\mathcal{M}_4^-\rvert^2 + \lvert\mathcal{M}_4^+\rvert^2$	
$I_0\,I^{s}$	$-2\,\Im\,(\mathcal{M}_1^+\,\mathcal{M}_1^{-\,*} + \mathcal{M}_2^+\,\mathcal{M}_2^{-\,*} + \mathcal{M}_3^+\,\mathcal{M}_3^{-\,*} + \mathcal{M}_4^+\,\mathcal{M}_4^{-\,*})$	linearly polarized photons, proportional to $\sin 2\beta$ in cross section
$I_0\,P_x^{s}$	$-2\,\Im\,(\mathcal{M}_1^+\,\mathcal{M}_3^{-\,*} - \mathcal{M}_1^-\,\mathcal{M}_3^{+\,*} + \mathcal{M}_2^+\,\mathcal{M}_4^{-\,*} - \mathcal{M}_2^-\,\mathcal{M}_4^{+\,*})$	
$I_0\,P_y^{s}$	$2\,\Re\,(-\mathcal{M}_1^+\,\mathcal{M}_3^{-\,*} + \mathcal{M}_1^-\,\mathcal{M}_3^{+\,*} - \mathcal{M}_2^+\,\mathcal{M}_4^{-\,*} + \mathcal{M}_2^-\,\mathcal{M}_4^{+\,*})$	
$I_0\,P_z^{s}$	$2\,\Im\,(\mathcal{M}_1^+\,\mathcal{M}_1^{-\,*} + \mathcal{M}_2^+\,\mathcal{M}_2^{-\,*} - \mathcal{M}_3^+\,\mathcal{M}_3^{-\,*} + \mathcal{M}_4^+\,\mathcal{M}_4^{-\,*})$	
$I_0\,I^{c}$	$-2\,\Re\,(\mathcal{M}_1^+\,\mathcal{M}_1^{-\,*} + \mathcal{M}_2^+\,\mathcal{M}_2^{-\,*} + \mathcal{M}_3^+\,\mathcal{M}_3^{-\,*} + \mathcal{M}_4^+\,\mathcal{M}_4^{-\,*})$	linearly polarized photons, proportional to $\cos 2\beta$ in cross section
$I_0\,P_x^{c}$	$-2\,\Re\,(\mathcal{M}_1^+\,\mathcal{M}_3^{-\,*} + \mathcal{M}_1^-\,\mathcal{M}_3^{+\,*} + \mathcal{M}_2^+\,\mathcal{M}_4^{-\,*} + \mathcal{M}_2^-\,\mathcal{M}_4^{+\,*})$	
$I_0\,P_y^{c}$	$2\,\Im\,(\mathcal{M}_1^+\,\mathcal{M}_3^{-\,*} + \mathcal{M}_1^-\,\mathcal{M}_3^{+\,*} + \mathcal{M}_2^+\,\mathcal{M}_4^{-\,*} + \mathcal{M}_2^-\,\mathcal{M}_4^{+\,*})$	
$I_0\,P_z^{c}$	$2\,\Re\,(\mathcal{M}_1^+\,\mathcal{M}_1^{-\,*} + \mathcal{M}_2^+\,\mathcal{M}_2^{-\,*} - \mathcal{M}_3^+\,\mathcal{M}_3^{-\,*} - \mathcal{M}_4^+\,\mathcal{M}_4^{-\,*})$	

Table 8: **Polarization observables of double-pion production**
Polarization observables of double-pion photoproduction in terms of helicity amplitudes [88]. Listed are observables for single and double-polarization experiments. In general, there are 64 polarization observables including the polarization measurement of the recoiling nucleon. Among the 64 observables, there are 28 relations that arise from consideration of the absolute magnitudes of the helicity amplitudes and another 21 that arise from considerations of their phases, leaving 15 independent quantities.

References

[1] U. Thoma, H. van Pee, and A. Sarantsev, *"Measurement of Double Polarisation Observables in $2\pi^0$-Photoproduction with the Crystal Barrel Detector at ELSA"*, 2005, ELSA Proposal ELSA/06-2005.

[2] F. Klein, T. Todor, and P. Eugenio, *"Search for Missing Nucleon Resonances in the Photoproduction of Hyperons using Polarized Photon Beam and Polarizd Target"*, 2002, JLab Proposal E02-112.

[3] S. Strauch, N. Benmouna, and I. Strakovsky, *"Pion Production From a Polarized Target"*, 2003, JLab Proposal E03-105.

[4] D. Sober, M. Khandaker, and D. Crabb, *"Helicity Structure of Pion Photoproduction"*, 2004, JLab Proposal E04-102.

[5] E. Pasyuk and M. Dugger, *"Measurement of polarization observables in η photoproduction with CLAS"*, 2005, JLab Proposal E05-012.

[6] J. Sanabria, J. Kellie, and F. Klein, *"Photoproduction of Associated Strangeness using a Linearly-Polarized Beam of Photons"*, 2001, CLAS Approved Analysis.

[7] P. Cole and K. Livingston, *"Photoproduction of ρ Mesons from the Proton with Linearly-Polarized Photons"*, 1994, JLab Proposal E94-109.

[8] D. Tedeschi, P. Cole, and J. Mueller, *"Photoproduction of ϕ Mesons with Linearly-Polarized Photons"*, 1998, JLab Proposal E98-109.

[9] F. Klein and P. Cole, *"Photoproduction of ω Mesons off Protons with Linearly-Polarized Photons"*, 1999, JLab Proposal E99-013.

[10] S. Capstick and N. Isgur, *"Baryons in a Relativized Quark Model with Chromodynamics"*, Phys. Rev. **D34**, 2809 (1986).

[11] L. Glozman and D. Riska, *"The Spectrum of the nucleons and the strange hyperons and chiral dynamics"*, Phys. Rept. **268**, 263 (1996), hep-ph/9505422.

[12] U. Loring, K. Kretzschmar, B. Metsch, and H. Petry, *"Relativistic quark models of baryons with instantaneous forces"*, Eur. Phys. J. **A10**, 309 (2001), hep-ph/0103287.

[13] K. Hagiwara *et al.*, [Particle Data Group], *"Review of particle physics"*, Phys. Rev. **D66**, 010001 (2002).

[14] T. D. Cohen and L. Y. Glozman, *"Chiral multiplets versus parity doublets in highly excited baryons"*, Phys. Rev. **D65**, 016006 (2002), hep-ph/0102206.

[15] V. Crede and the CB-TAPS Collaboration, *"Parity Doublets in the Baryon Spectrum: Exploratory Studies with the CB–TAPS Detector at ELSA"*, 2002, PAC Proposal ELSA/2-2002.

[16] R. Plotzke *et al.*, [SAPHIR Collaboration], *"Photoproduction of η' mesons with the 4π-detector SAPHIR"*, Phys. Lett. **B444**, 555 (1998).

[17] W.-T. Chiang *et al.*, *"A reggeized model for η and η' photoproduction"*, Phys. Rev. **C68**, 045202 (2003), nucl-th/0212106.

[18] K. Glander *et al.*, [SAPHIR Collaboration], *"Measurement of $\gamma p \to K^+\Lambda$ and $\gamma p \to K^+\Sigma^0$ at photon energies up to 2.6 GeV"*, Eur. Phys. J. **A19**, 251 (2004), nucl-ex/0308025.

[19] C. Bennhold *et al.*, *"$K^0\,\Sigma^+$ photoproduction with SAPHIR"*, Nucl. Phys. **A639**, 209 (1998), nucl-th/9711048.

[20] R. Lawall *et al.*, *"Measurement of the reaction $\gamma p \to K^0\Sigma^+$ at photon energies up to 2.6 GeV"*, Eur. Phys. J. **A24**, 275 (2005), nucl-ex/0504014.

[21] J. W. C. McNabb *et al.*, [CLAS Collaboration], *"Hyperon Photoproduction in the Nucleon Resonance Region"*, Phys. Rev. **C69**, 042201 (2004), nucl-ex/0305028.

[22] R. G. T. Zegers *et al.*, [LEPS Collaboration], *"Beam polarization asymmetries for the $p(\gamma, K^+)\Lambda$ and $p(\gamma, K^+)\Sigma^0$ reactions at $E_\gamma = 1.5 - 2.4$ GeV"*, Phys. Rev. Lett. **91**, 092001 (2003), nucl-ex/0302005.

[23] A. V. Sarantsev *et al.*, *"Decays of baryon resonances into ΛK^+, $\Sigma^0 K^+$ and $\Sigma^+ K^0$"*, (2005), hep-ex/0506011.

[24] V. Crede *et al.*, [CB–ELSA Collaboration], *"Photoproduction of η mesons off protons for $0.75\ GeV < E_\gamma < 3\ GeV$"*, Phys. Rev. Lett. **94**, 012004 (2005), hep-ex/0311045.

[25] O. Bartholomy *et al.*, [CB–ELSA Collaboration], *"Neutral pion photoproduction off protons in the energy range $0.3\ GeV < E_\gamma < 3\ GeV$"*, Phys. Rev. Lett. **94**, 012003 (2005), hep-ex/0407022.

[26] V. I. Mokeev *et al.*, *"Phenomenological model for describing pion pair production on a proton by virtual photons in the energy region of nucleon resonance excitation"*, Phys. Atom. Nucl. **64**, 1292 (2001).

[27] S. Capstick, *"Photoproduction and electroproduction of nonstrange baryon resonances in the relativized quark model"*, Phys. Rev. **D46**, 2864 (1992).

[28] O. Krehl, C. Hanhart, S. Krewald, and J. Speth, *"What is the structure of the Roper resonance?"*, Phys. Rev. **C62**, 025207 (2000), nucl-th/9911080.

[29] Z.-p. Li, V. Burkert, and Z.-j. Li, *"Electroproduction of the Roper resonance as a hybrid state"*, Phys. Rev. **D46**, 70 (1992).

[30] J. Gomez Tejedor and E. Oset, *"Double pion photoproduction on the nucleon: Study of the isospin channels"*, Nucl. Phys. **A600**, 413 (1996), hep-ph/9506209.

[31] L. Murphy and J. Laget, 1996, "DAPHNIA/SPhN 96–10".

[32] M. Bellis, private communication.

[33] A. Braghieri *et al.*, *"Total cross section measurement for the three double pion production channels on the proton"*, Phys. Lett. **B363**, 46 (1995).

[34] W. Langgartner *et al.*, *"Direct observation of a ρ decay of the $D_{13}(1520)$ baryon resonance"*, Phys. Rev. Lett. **87**, 052001 (2001).

[35] M. Kotulla, Phd thesis, University of Gießen, 2001, unpublished.

[36] E. Hourany, AIP Conf. Proc. **610**, 362 (2001), INPC 2001.

[37] B. Krusche and S. Schadmand, *"Study of non–strange baryon resonances with meson photoproduction"*, Prog. Part. Nucl. Phys. **51**, 399 (2003), nucl-ex/0306023.

[38] [ABBHHM Collaboration], Phys. Rev. **175**, 1669 (1968).

[39] G. Gialanella *et al.*, Nuovo Cimento **A LXIII**, 892 (1969).

[40] A. Piazza *et al.*, Lett. Nuovo Cimento **III**, 403 (1970).

[41] C. B. C. Group, Phys. Rev. **155**, 1477 (1967).

[42] C. B. C. Group, Phys. Rev. **163**, 1510 (1967).

[43] H. Crouch *et al.*, Phys. Rev. Lett. **13**, 636 (1964).

[44] H. Hilpert *et al.*, Phys. Lett. **23**, 707 (1966).

[45] G. Audit *et al.*, *"DAPHNE: a large-acceptance tracking detector for the study of photoreactions at intermediate energies"*, Nucl. Instrum. Meth. **A301**, 473 (1991).

[46] R. Novotny, [TAPS Collaboration], *"The BaF two-photon spectrometer TAPS"*, IEEE Trans. Nucl. Sci. **38**, 379 (1991).

[47] A. Gabler *et al.*, *"Response of TAPS to monochromatic photons with energies between 45 MeV and 790 MeV"*, Nucl. Instrum. Meth. **A346**, 168 (1994).

[48] F. Harter *et al.*, *"Two neutral pion photoproduction off the proton between threshold and 800 MeV"*, Phys. Lett. **B401**, 229 (1997).

[49] A. Zabrodin *et al.*, *"Total cross section measurement of the $\gamma\, n \to p\, \pi^-\, pi^0$ reaction"*, Phys. Rev. **C55**, 1617 (1997).

[50] A. Zabrodin *et al.*, *"Invariant mass distributions of the $\gamma\, n \to p\, \pi^-\, \pi^0$ reaction"*, Phys. Rev. **C60**, 055201 (1999).

[51] M. Wolf *et al.*, *"Photoproduction of neutral pion pairs from the proton"*, Eur. Phys. J. **A9**, 5 (2000).

[52] V. Kleber *et al.*, *"Double π^0 photoproduction from the deuteron"*, Eur. Phys. J. **A9**, 1 (2000).

[53] F. Klein, Phd thesis, University of Bonn, 1996, BONN-IR-96-08.

[54] U. Thoma, *"The search for missing baryon resonances"*, (2005), nucl-ex/0501007.

[55] D. Luke and P. Soding, Springer Tracts in Modern Physics **59**, 39 (1971).

[56] K. Ochi, M. Hirata, and T. Takaki, *"Photoabsorption on a nucleon in the D_{13} resonance energy region"*, Phys. Rev. **C56**, 1472 (1997), nucl-th/9703058.

[57] J. Gomez Tejedor, F. Cano, and E. Oset, *"The $N^*(1520) \to \Delta\, \pi$ Amplitudes Extracted from the $\gamma\, p \to \pi^+ \pi^-\, p$ Reaction and Comparison to Quark Models"*, Phys. Lett. **B379**, 39 (1996), nucl-th/9510007.

[58] M. Ripani, *"Pentaquarks: The experimental situation"*, Prepared for 16th Conference on High Energy Physics (IFAE 2004), Turin, Italy, 14-16 Apr 2004.

[59] Prepared for NSTAR 2004 Workshop on the Physics of Excited Nucleons, Grenoble, France, 24-27 Mar 2004.

[60] M. Ripani *et al.*, [CLAS Collaboration], *"Measurement of $e\,p \to e'\,p\,\pi^+\pi^-$ and baryon resonance analysis"*, Phys. Rev. Lett. **91**, 022002 (2003), hep-ex/0210054.

[61] I. G. Aznauryan, V. D. Burkert, G. V. Fedotov, B. S. Ishkhanov, and V. I. Mokeev, *"Electroexcitation of nucleon resonances at $Q^2 = 0.65$ $GeV/c)^2$ from a combined analysis of single- and double- pion electroproduction data"*, Phys. Rev. **C72**, 045201 (2005), hep-ph/0508057.

[62] Y. Assafiri *et al.*, *"Double π^0 photoproduction on the proton at GRAAL"*, Phys. Rev. Lett. **90**, 222001 (2003).

[63] A. Anisovich, E. Klempt, A. Sarantsev, and U. Thoma, *"Partial wave decomposition of pion and photoproduction amplitudes"*, (2004), hep-ph/0407211.

[64] J. Ahrens *et al.*, [GDH and A2 Collaboration], *"Helicity dependence of the $\vec{\gamma}\,\vec{p} \to n\,\pi^+\pi^0$ reaction in the second resonance region"*, Phys. Lett. **B551**, 49 (2003).

[65] J. Nacher, E. Oset, M. Vicente, and L. Roca, *"The role of $\Delta(1700)$ excitation and ρ production in double pion photoproduction"*, Nucl. Phys. **A695**, 295 (2001), nucl-th/0012065.

[66] J. Nacher and E. Oset, *"Study of polarization observables in double pion photoproduction on the proton"*, Nucl. Phys. **A697**, 372 (2002), nucl-th/0106005.

[67] S. Strauch *et al.*, [CLAS Collaboration], *"Beam-Helicity Asymmetries in Double-Charged-Pion Photoproduction on the Proton"*, Phys. Rev. Lett. **95**, 162003 (2005),

[68] V. Burkert *et al.*, Nucl. Phys. **A737**, S231 (2004).

[69] A. Fix and H. Arenhovel, *"Double pion photoproduction on nucleon and deuteron"*, Eur. Phys. J. **A25**, 115 (2005), nucl-th/0503042.

[70] V. Burkert *et al.*, *"New Possibilities for Studying Nucleon Resonances on the Basis of an Analysis of Polarization Observables and Off-Scattering-Plane Angular Distributions in the Reaction $\gamma_v p \to \pi^+\pi^- p$"*, Phys. Atom. Nucl. **66**, 2149 (2003).

[71] V. I. Mokeev *et al.*, *"Helicity Components of the Cross Section for Double Charged-Pion Production by Real Photons on Protons"*, Phys. Atom. Nucl. **66**, 1282 (2003).

[72] L. Roca, *"Helicity asymmetries in double pion photoproduction on the proton"*, Nucl. Phys. **A748**, 192 (2005), nucl-th/0407049.

[73] W. Roberts and A. Rakotovao, *"A model for two-pion photoproduction amplitudes"*, (1997), hep-ph/9708236.

[74] S. Eidelman *et al.*, [Particle Data Group], *"Review of particle physics"*, Phys. Lett. **B592**, 1 (2004).

[75] S. Capstick and W. Roberts, *"Quasi two-body decays of nonstrange baryons"*, Phys. Rev. **D49**, 4570 (1994), nucl-th/9310030.

[76] G. Hohler *et al.*, Handbook of Pion–Nucleon Scattering, Physics Data **12–1** (1979).

[77] R. Cutkosky, C. Forsyth, R. Hendrick, and R. Kelly, *"PION - NUCLEON PARTIAL WAVE AMPLITUDES"*, Phys. Rev. **D20**, 2839 (1979).

[78] D. Manley and E. Saleski, *"Multichannel resonance parametrization of πN scattering amplitudes"*, Phys. Rev. **D45**, 4002 (1992).

[79] S. Capstick and W. Roberts, *"$N\pi$ decays of baryons in a relativized model"*, Phys. Rev. **D47**, 1994 (1993).

[80] D. Sober *et al.*, *"The bremsstrahlung tagged photon beam in Hall B at JLab"*, Nucl. Instrum. Meth. **A440**, 263 (2000).

[81] H. Olsen and L. Maximon, Phys. Rev. **114**, 887 (1959).

[82] W. Meyer, Prepared for Symposium on the Gerasimov-Drell-Hearn Sum Rule and the Nucleon Spin Structure in the Resonance Region (GDH 2000), Mainz, Germany, 14-17 Jun 2000.

[83] C. Bradtke *et al.*, *"A new frozen–spin target for 4π particle detection"*, Nucl. Instrum. Meth. **A436**, 430 (1999).

[84] C. Dzyubak, O. Djalali and D. Tedeschi, 2004, "CLAS Note 2004–023 (2004) (http://www.jlab.org/Hall–B/notes/clas_notes04/2004–023.pdf)".

[85] J. Billen and L. Young, *"POISSON/SUPERFISH"*, 2003, LANL Report LA–UR–96–1834 (revised April 2003).

[86] *"OPERA–3D User Guide"* (Vector Fields Ltd., England, 2002), F–01–02–D2.

[87] O. Dzyubak, C. Djalali, N. Recalde, and D. Tedeschi, *"Design of internal superconducting holding magnet for the JLAB Hall-B frozen spin polarized target"*, Nucl. Instrum. Meth. **A526**, 132 (2004).

[88] W. Roberts and T. Oed, *"Polarization Observables for Two-Pion Production off the Nucleon"*, (2004), nucl-th/0410012.

[89] C. Wu *et al.*, [SAPHIR Collaboration], *"Photoproduction of ρ^0 mesons and Δ baryons in the reaction $\gamma p \to p\pi^+\pi^-$ at energies up to $\sqrt{s} = 2.6$ GeV"*, Eur. Phys. J. **A23**, 317 (2005).

[90] S. Chung, *"Helicity coupling amplitudes in tensor formalism"*, Phys. Rev. **D48**, 1225 (1993).

[91] W. Rarita and J. Schwinger, *"On a theory of particles with half integral spin"*, Phys. Rev. **60**, 61 (1941).

[92] D. Drechsel and L. Tiator, *"Threshold pion photoproduction on nucleons"*, J. Phys. **G18**, 449 (1992).

[93] G. Knochlein, D. Drechsel, and L. Tiator, *"Photoproduction and electroproduction of η mesons"*, Z. Phys. **A352**, 327 (1995), nucl-th/9506029.

[94] M. Williams, *"Covariant Partial Wave Formalism for Baryon Photoproduction Amplitudes"*, 2003, unpublished.

[95] W. Roberts, private communication.